AMERICAN
METEOROLOGICAL
SOCIETY

Journal of Climate

The DOI for this manuscript is doi: 10.1175/JCLI-D-11-00649.1

The final published version of this manuscript will replace the preliminary version at the above DOI once it is available.

If you would like to cite this EOR in a separate work, please use the following full citation:

Gergis, J., R. Neukom, S. Phipps, A. Gallant, and D. Karoly, 2012: Evidence of unusual late 20th century warming from an Australasian temperature reconstruction spanning the last millennium. J. Climate. doi:10.1175/JCLI-D-11-00649.1, in press.

Evidence of unusual late 20th century warming from an Australasian temperature reconstruction spanning the last millennium

Joëlle Gergis[1], Raphael Neukom[1], Steven J. Phipps[2, 3], Ailie J.E. Gallant[1], David J. Karoly[1]

and PAGES Aus2K Project Members†

[1] School of Earth Sciences, University of Melbourne, Australia

[2] Climate Change Research Centre, University of New South Wales, Sydney, Australia

[3]ARC Centre of Excellence for Climate System Science, University of New South Wales, Sydney, Australia

Corresponding author

Dr Joëlle Gergis
School of Earth Sciences
University of Melbourne,
VIC 3010, AUSTRALIA
Ph: +61 3 834 49868
Fax: +61 3 834 47761
Mobile: + 61 415 449 241

Email: jgergis@unimelb.edu.au

Manuscript submitted to *Journal of Climate*

† Aus2K project member data and other contributions from Kathryn Allen, Patrick Baker, Gretel Boswijk, Brendan Buckley, Matthew Brookhouse, Edward Cook, Louise Cullen, Mark Curran, Rosanne D'Arrigo, Pavla Fenwick, Anthony Fowler, Ian Goodwin, Pauline Grierson, Erica Hendy, Braddock Linsley, Janice Lough, Andrew Lorrey, Helen McGregor, Andrew Moy, Jonathan Palmer, Christopher Plummer, Chris Turney, Tessa Vance, Tas Van Ommen and Limin Xiong.

Abstract

This study presents the first multi-proxy warm season (September–February) temperature reconstruction for the combined land and oceanic region of Australasia (0ºS–50ºS, 110ºE–180ºE). We perform a 3000-member ensemble Principal Component Reconstruction (PCR) using 27 temperature proxies from the region. The proxy network explained 69% of the inter-annual variance in the HadCRUT3v SONDJF spatial mean temperature over the 1921–1990 calibration period. Applying eight stringent reconstruction 'reliability' metrics identified post A.D. 1430 as the highest quality section of the reconstruction, but also revealed a skilful reconstruction is possible over the full A.D. 1000–2001 period.

The average reconstructed temperature anomaly in Australasia during A.D. 1238–1267, the warmest 30-year pre-instrumental period, is 0.09°C (±0.19°C) below 1961–1990 levels. Following peak pre-industrial warmth, a cooling trend culminates in a temperature anomaly of 0.44°C (±0.18°C) below 1961–1990 levels between A.D. 1830–1859. A preliminary assessment of the roles of solar, volcanic, and anthropogenic forcings and natural ocean–atmosphere variability is performed using CSIRO Mk3L model simulations and independent palaeoclimate records. Solar and volcanic forcing does not have a marked influence on reconstructed Australasian temperature variations, which appear to be masked by internal variability.

In 94.5% of the 3000-member reconstruction ensemble, there are no other warm periods in the past 1,000 years that match or exceed post-1950 warming observed in Australasia. The unusual 20th century warming cannot be explained by natural variability alone, suggesting a strong influence of anthropogenic forcing in the Australasian region.

Keywords: temperature, Australasia, palaeoclimate reconstruction, last millennium, climate forcing, climate variability, climate change.

1. Introduction

Palaeoclimate records are fundamental in evaluating the long term context of recent regional and global climate variability. Extending our baseline of pre-industrial climate variations from climate proxies allows natural or internal variations to be isolated from anthropogenically forced changes using detection and attribution studies (Hegerl *et al.*, 2011). Uncertainties in future climate change projections depend not only on future emissions of greenhouse gases, but also on the ability of climate models to skilfully simulate past climate variability. Reconstructions of regional-scale temperature provide an extended basis for evaluating the accuracy of climate models in simulating past regional climate variability and an opportunity to reduce uncertainties associated with future climate variability and change (Hegerl et al., 2006; Hegerl et al., 2011).

In this study we consider the land and ocean region of Australasia, an area of Oceania comprising Australia, New Zealand and neighbouring islands in the Indian, Southern and Pacific Oceans bounded by 110^{o}E–180^{o}E and 0^{o}S–50^{o}S. Multi-decadal warming has been observed across much of Australasia as far back as the beginning of the 20th century. Since 1910 (the period of extensive high-quality observational records), Australia, the largest continental mass in Australasia, has experienced an annual mean land surface temperature increase of 0.9°C with approximately 0.7ºC of the warming observed since 1960 (Della-Marta *et al.*, 2004; Keenan and Cleugh, 2011). 2001–2010 was the warmest decade recorded in both Australian land and sea surface temperature (SST) observations (Keenan and Cleugh, 2011). Increases in mean minimum and maximum temperatures have also been observed from stations on the north and south islands of New Zealand over the period 1961–2005 (Chambers and Griffiths, 2008). Recent work has found that the late 20th century and early 21st century (1980–2009) warming of Australian waters was 0.57ºC higher than the early 20th century SSTs (1910–1939), with greatest increases reported off the south-eastern and south-western Australian coasts (Lough and Hobday, 2011).

Given the large warming trend observed in Australasian temperature records since the late 20th century, it is important to understand how regional climate in the region has fluctuated in pre-industrial times – centuries before meteorological observations become available – and test how these palaeoclimate estimates can be used to evaluate climate model projections in this region. Current model projections suggest that Australian temperatures may rise between 0.7ºC–1.2ºC above 1990 levels by 2030, with a best estimate of 1ºC (CSIRO, 2007). Increases of 1–5ºC by 2070 are projected over various regions of Australia dependent on global greenhouse gas mitigation policies, with a best estimate of 1.8–3.4ºC (CSIRO, 2007). Robust, well-verified palaeoclimate reconstructions can help evaluate global climate models relied upon by natural resource managers to plan for future climate change in the Australasian region by providing better estimates of decadal scale climate variations.

Reconstructions of past climate variability from Australasia are not only regionally important but contain core dynamical regions of several major atmospheric and oceanic circulation features that have a hemispheric or near-global influence e.g. El Niño–Southern Oscillation (ENSO), Inter-decadal Pacific Oscillation (IPO), Southern Annular Mode (SAM), Australian Monsoon, Indian Ocean Dipole, and the mid-latitude westerlies. Reconstructing past variations in the Australasian region therefore allows us to estimate the variability in these major climate modes associated with both natural and anthropogenic forcings. Ultimately this will allow us to better predict the evolution of these circulation features and their regional climatic impacts.

Northern Hemisphere multi-proxy temperature reconstructions show that recent warmth appears anomalous for at least the past 1,300 years (Jansen *et al.*, 2007; Mann *et al.*, 2008). The multi-proxy temperature reconstructions that are currently available for Southern Hemisphere (Jones *et al.*, 1998; Huang *et al.*, 2000; Mann and Jones, 2003; Mann *et al.*, 2008) are considerably more uncertain due to the limited availability of long proxy records and hitherto lack of consolidation of available records from the region (Neukom and Gergis, 2011). Huang *et al.*’s (2000) centennially-resolved borehole estimates from Australia, South America and Africa indicate that the magnitude of land surface warming over the past 500 years is estimated to be less in the Southern Hemisphere locations (0.8^{o}C) than the Northern Hemisphere (1.1^{o}C).

Despite advances in estimating hemispheric and global mean temperature trends over the last 2,000 years (Wahl *et al.*, 2010), there are still considerable uncertainties in understanding regional responses to large-scale temperature changes from global radiative forcing (D'Arrigo *et al.*, 2009; Mann *et al.*, 2009). Little is known about the magnitude and timing of temperature fluctuations in Southern Hemisphere regions during the so-called 'Medieval Climate Anomaly' (MCA) warm (A.D. 900–1250) or 'Little Ice Age' (LIA) cool (A.D.1400–1700) intervals described from Northern Hemisphere climate reconstructions (Hughes and Diaz, 1994; D'Arrigo *et al.*, 2009; Mann *et al.*, 2009; Diaz *et al.*, 2011; Graham *et al.*, 2011).

The IPCC AR4 section on climate of the last 2,000 years in the Australasian region (Jansen *et al.*, 2007) focused on two annually-resolved tree ring-based land temperature reconstructions from Australia and New Zealand, and a composite of 57 centennially-resolved borehole sites throughout Australia (Cook et al., 2000; Cook et al., 2002a; Pollack et al., 2006). Silver Pine tree ring widths from New Zealand suggest that 20th century warm season temperatures have been unusual, but not unprecedented in the context of the past millennium in this sub region of Australasia (D'Arrigo et al., 1998; Cook et al., 2002a; Cook et al., 2002b; Cook et al., 2006). For instance, two periods of above average warmth are recorded in the western South Island Silver Pine record in the medieval period around A.D.1137–1177 and 1210–1260. This represents temperatures 0.3–0.5^{o}C higher than the 1894–1998 average calibrated from the single station record of Hokitika (Cook et al., 2002b), but is within the 0.4–0.7°C range of abrupt instrumental warming observed in the anthropogenically-influenced period in the west coast of the South Island of New Zealand since 1950 (Hennessy *et al.*, 2007).

In contrast, the Huon Pine tree ring reconstructed temperature record from western Tasmania in Australia shows more pronounced regional warming associated with warming of Indian and Southern Ocean sea surface temperatures from around 1965 until the end of the record in 2001 (Cook *et al.*, 2000; Cook *et al.*, 2006). Over the past 2,000 years the temperature reconstruction suggests that late 20th century temperatures were only exceeded by ~0.28^{o}C for three short periods, around 455 BC, 380 BC and AD 10 (Cook *et al.*, 2006). They conclude that late 20th century warming is unprecedented over the past 2,000 years in Tasmania and highly anomalous when viewed in the context of the past 3,602 years (Cook *et al.*, 2006).

The unusual nature of recent warmth is also suggested by a composite borehole temperature reconstruction for Australia which shows a temperature increase of approximately 0.5^{o}C over the past 500 years, with 80% of the warming occurring during the 19th and 20th centuries (Pollack *et al.*, 2006). The record indicates that the 17th century was the coolest interval of the five-century reconstruction. Because most of the Australian boreholes were logged prior to 1976, the observed subsurface temperatures do not include the pronounced warming recorded over the last two decades of the 20th century, but currently provide the only baseline of pre-industrial temperature conditions experienced over the large-scale continental region of Australia (Pollack *et al.*, 2006; Jansen *et al.*, 2007).

In recent years, attention has expanded to quantifying regional temperature variations in palaeoclimate reconstructions in response to the radiative forcing associated with natural solar and volcanic variations, and increases in anthropogenic greenhouse gases concentrations (Mann *et al.*, 2005; Hegerl *et al.*, 2007b). In particular, there has been a focus on improving climate reconstructions of the last 2000 years as it is a period that contains marked temperature variations in many parts of the globe like the MCA, LIA and late 20th century warming (Jones and Mann, 2004; Jones *et al.*, 2009), and is the period when the majority of the Earth's precisely dated, high-resolution palaeoclimate records are available for direct calibration with instrumental records.

In response to the lack of continental-scale climate reconstructions in the IPCC AR4, in 2009 the International Geosphere–Biosphere Programme's (IGBP) Past Global Changes (PAGES) initiative developed the Regional 2k Network, a set of working groups to collect and process the best available proxy data to develop climate reconstructions in eight regions of the world (http://www.pages-igbp.org/workinggroups/2k-network; Newman *et al.*, 2009). The Australasia (Aus2k) working group is examining the Indo–Pacific region consisting of the landmasses of

Australia, New Zealand, the Indonesian archipelago and the neighbouring islands of the Pacific Ocean.

This paper is the Aus2k working group's regional consolidation of temperature proxies to provide a 'best estimate' of Australasian temperature variations over the past 1000 years. We present the development of the region's first multi-proxy combined land and ocean mean temperature reconstruction for the austral spring–summer (SONDJF) warm season. We assess multi-decadal temperature variations present in the reconstruction, and then identify extreme cool and warm periods to assess the long-term context of the anomalous late 20th century warming seen in observational records. Finally, we compare our results with 1000-year forced and unforced CSIRO MK3L climate model simulations. This provides a preliminary investigation of the importance of natural forcing, anthropogenic forcing and internal climate variability for Australasian temperature fluctuations over the past millennium and demonstrates the value of such reconstructions for detection and attribution studies.

2. Data and methods

2.1. Instrumental calibration data

In this study, Australasia is defined as the land and ocean areas of the Indo–Pacific and Southern Oceans bounded by 110^{o}E–180^{o}E, 0^{o}–50^{o}S. Our instrumental target was calculated as the September–February (SONDJF) spatial mean of the HadCRUT3v 5^{o} x 5^{o} monthly combined land and ocean temperature grid (Brohan *et al.*, 2006; Rayner *et al.*, 2006) for the Australasian domain over the 1900–2009 period. The SONDJF seasonal window correlates highly with the MAMJJA season (r=0.87) and the annual mean (r=0.93) on inter-annual timescales over the 1900–2010 period. Since the HadCRUT3v grid contains significant amounts of missing data in the pre-1900 period across the region, the 1850–1899 section was excluded from our analysis (Jones *et al.*, 1999; Brohan *et al.*, 2006).

To assess the large-scale coherence of land and ocean temperatures over the broad Australasian region, we performed a correlation analysis to identify all HadCRUT3v grid cells displaying a significant positive correlation with the predictand over the 1900–1990 period (Figure S1). This analysis revealed a high degree of spatial coherence of warm season temperatures over the Australasian region with the exception of areas in Western Australia containing missing values, parts of south east Asia influenced by local monsoon variability, the data sparse region of the Southern Ocean, and the mountainous area of eastern Australia. Overall, 73% of grid cells (100 out of 137) were significantly positively correlated ($p<0.05$) with the Australasian spatial mean (Figure S1). This result is not surprising as the flat, arid continent of Australia and its surrounding ocean dominates the majority of Australasian, confirming that reconstructing a spatial mean of coherent temperature over the region is an acceptable approach for the region.

2.2. Temperature predictor network

Our temperature proxy network was drawn from a broader Australasian domain (90^{o}E–140^{o}W, 10^{o}N–80^{o}S) containing 62 monthly–annually resolved climate proxies from approximately 50 sites (see details provided in Neukom and Gergis, 2011). This proxy network showed optimal response to Australasian temperatures over the SONDJF period, and contains the austral tree ring growing season during the spring–summer months. All tree ring chronologies were developed based on raw measurements using the signal-free detrending method (Melvin *et al.*, 2007; Melvin and Briffa, 2008). All years where less than five tree ring series were available or Expressed Population Signal (EPS; Briffa and Jones, 1990) values were below 0.85 were excluded from the analysis.

The only exceptions to this signal-free tree ring detrending method was the New Zealand Silver Pine tree ring composite (Oroko Swamp and Ahaura), which contains logging disturbance after 1957 (D'Arrigo et al., 1998; Cook et al., 2002a; Cook et al., 2006) and the Mount Read Huon Pine chronology from Tasmania which is a complex assemblage of material derived from living trees and sub-fossil material. For consistency with published results, we use the final temperature reconstructions provided by the original authors that includes disturbance-corrected data for the Silver Pine record and Regional Curve Standardisation for the complex age structure of the wood used to develop the Mount Read temperature reconstruction (E. Cook, personal communication, Cook et al., 2006).

Although the Mount Read record from Tasmania extends as long as 3602 years, in this study we only examine data spanning the last 1000 years which contains the better replicated sections of the Silver Pine chronology from New Zealand (Cook et al., 2002b; Cook et al., 2006) and is the key period for which model simulations have been run for comparison with palaeoclimate reconstructions (e.g. Schmidt *et al.*, 2012).

All coral records with monthly, bimonthly or seasonal resolution were averaged over the SONDJF period to align with the warm season reconstruction window. For predictor selection, both proxy climate and instrumental data were linearly detrended over the 1921–1990 period to avoid inflating the correlation coefficient due to the presence of the global warming signal present in the observed temperature record. Only records that were significantly ($p<0.05$) correlated with the detrended instrumental target over the 1921–1990 period were selected for analysis. This process identified 27 temperature-sensitive predictors for the SONDJF warm season (Figure 1 and Table 1) henceforth referred to as R27. Missing values in the predictor matrix during the calibration period (0.4%) were infilled using principal component regression (Scherrer and Appenzeller, 2006; Neukom *et al.*, 2011).

2.3. Ensemble reconstruction method and verification

We performed an ensemble ordinary least squares regression Principal Component Reconstruction (PCR) analysis (Neukom *et al.*, 2010; Gallant and Gergis, 2011; Gergis *et al.*, 2012) using the 1921–1990 period for calibration and verification. Further description of the PCR method is provided by Luterbacher *et al.* (2002), and details of the extension of the ensemble approach are described below. To assess reconstruction uncertainty associated with proxy selection and calibration, a 3000-member ensemble of reconstructions was calculated creating varying reconstruction setting for each realisation by randomly:

- Removing five predictors from the full predictor matrix. In the early part of the reconstruction (1000–1456) where five or fewer proxies are available, the number of predictors used for each ensemble member varies between one and five. The effect of varying the number of proxies to be removed is illustrated in Figures S2.4 and S2.5.
- Varying the percentage of total variance of the predictor matrix explained by the retained PCs between 60% and 90% by varying the number of PCs used.
- Selecting a calibration period of 35–50 (non successive) years between 1921–1990 and using the remaining 20–35 years for verification.
- Scaling the weight of each proxy record in the PC analysis with a factor of 0.67 to 1.5. The effect of varying the weighting factor is illustrated in Figures S2.6 and S2.7.

To avoid variance biases due to the decreasing number of predictors back in time, the reconstructions of each model were scaled to the variance of the instrumental target over the 1921–1990 period. The mean of the 3,000-member ensemble was considered our 'best estimate' temperature reconstruction. To assess low frequency changes in Australasian temperatures, the ensemble mean was smoothed using a 30-year loess filter (Figure 3), which effectively removes variations with periods shorter than 15 years. To assess the influence of the loss of climate proxies back in time we also compare results from the R27 (all proxies), R21 (pre-1801 proxies), R14 (pre-1701 proxies) and R4 (pre-1458 proxies) networks (see supplementary section S2).

The ensemble PCR method allows us to quantify not only the traditional regression residual-based uncertainties referred to as 'calibration error' (e.g. Cook and Kairiukstis, 1990), but also the spread of the ensemble members generated from the random selection of the reconstruction parameters, described as the 'ensemble error'. The reconstruction confidence interval was defined as the combined calibration and ensemble standard error (SE), calculated as $SE = \sqrt{\sigma_{res}^2 + \sigma_{ens}^2}$ with σ_{res} denoting the standard deviation of the regression residuals and σ_{ens} the standard deviation of the ensemble members. Uncertainties of the filtered curves were calculated the same way using the residuals of the filtered data and standard deviation between the filtered ensemble members.

In addition to the 3,000 verification tests incorporated into the 1921–1990 overlap period calculations, the ensemble mean was also further independently verified using withheld, early 1901–1920 data (‘early verification’). Reconstruction ‘reliability’ was assessed using a set of eight skill and robustness metrics for each year back in time (Table S6). Skill measures included the calculation of mean Reduction of Error (RE), Root Mean Square Error (RMSE) and comparison with reconstructions developed using random noise proxies. ‘Skilful’ years were identified when the ensemble median RE (RMSE of the ensemble mean) was larger (smaller) than the corresponding values of a reconstruction using AR1 noise predictors. If our predictor network performed better than pure noise proxies, we assumed that our reconstruction is not simply a result of ‘overfitting’ noise in the calibration period (McShane and Wyner, 2011). Reconstruction ‘robustness’ was assessed on inter-annual and decadal timescales by investigating changes in the ensemble mean in response to changes in the predictor network or reconstruction ensemble parameters. Years where the 30-year filtered ensemble mean and the running inter-annual variance of the reconstruction did not change significantly with changes in the proxy network or ensemble, were considered robust.

We assessed three different kinds of changes in the proxy network or ensemble: (i) using all ensemble members vs. using only the ensemble members where a given proxy was excluded from the predictor set (and repeating this for all proxies); (ii) using all proxies vs. using only the proxies that are available at a given year (and repeating this for all years with different proxy availability); and (iii) using all ensemble members vs. using only the ensemble members with positive RE in each year. Applying these three tests on inter-annual as well as decadal timescales yields six robustness criteria.

Next, we undertook instrumental verification analyses to test whether we could reasonably reconstruct mean temperature from the whole Australasian field using instrumental data only from grid cells within the R27 proxy network. This was done by applying the above reconstruction method to instrumental data taken from the HadCRUT3v grid at locations closest to the 27 proxy locations over the 1921 to 2000 period. Large amounts of missing data in the HadCRUT3v grid in the early 20th century meant that only grids with less than 33.3% of data missing were used. For further validation, the same analysis was also run using instrumental temperatures from the closest Global Historical Climatology Network (GHCN) stations (Peterson and Vose, 1997) for land temperature proxies and the HadISST data (Rayner *et al.*, 2003) for ocean temperature proxies. Note that considerable amounts of missing data from a number of stations in our domain restricted the GHCN analysis to the 1953–1992 period.

As a final 'pseudo instrumental' verification exercise, ten different variants of the HadCRUT3v grid points were 'degraded' by including white noise so that the relationship (as measured by the Pearson correlation) between the degraded grid cell and the original grid cell was the same as that between the original grid cell and the proxy record. Since each proxy displays a different correlation coefficient with its corresponding observation, the amount of white noise added was correspondingly different at each location.

2.4. Climate model simulations

To assess the role of climate forcing on our 'best estimate' warm season Australasian temperature reconstruction over the past millennium, we compared our temperature reconstruction results to a three-member ensemble of the CSIRO Mk3L climate system model version 1.2, a fully coupled global atmosphere–ocean general circulation model (Phipps *et al.*, 2011; Phipps *et al.*, 2012). The model incorporates a 5.6 x 3.2 degree atmosphere with 18 vertical levels, a 2.8 x 1.6 degree ocean with 21 vertical levels, dynamic-thermodynamic sea ice and static vegetation and soil types (Phipps *et al.*, 2011). Three transient simulations are considered here which incorporate the effects of changes in orbital forcing, greenhouse gases (MacFarling–Meure *et al.*, 2006), solar irradiance (Steinhilber *et al.*, 2009) and volcanic aerosols (Gao *et al.*, 2008) over the last millennium (Phipps *et al.*, 2012). We also considered CSIRO Mk 3L 1000-year sections of a 10,000-year control run simulation to assess the relative roles of forced and unforced climate variations in driving changes in Australasian temperature changes over the past 1000 years.

Although there are a number of model simulations that are currently available, in this study we require the following two criterion be satisfied: i) availability of millennial length control simulations to adequately characterise internal or unforced climate variability and ii) a multi-member ensemble of 1000-year simulations forced with solar, volcanic and anthropogenic greenhouse gases to distinguish between unforced and forced climate variability. Currently there are very few Coupled Model Intercomparison Project (CMIP5) and Palaeoclimate Model Inter-comparison Project (PMIP3) climate models that have ensembles of simulations for the last millennium or extend past 1850 with a full suite of forcings. As such, we restrict our preliminary comparison of variations in 3000-member Australasian temperature reconstruction ensemble to the CSIRO Mk 3L model that has an ensemble of three simulations with the same forcings over the full period of our temperature reconstruction ensemble (A.D 1000–2001). This allows us to better estimate decadal variability due to internal noise from forced responses seen in the ensemble mean of the model simulations. For a more extensive comparison of the Australasian temperature reconstruction with climate model simulations, the reader is referred to Phipps *et al*. (2012).

3. Results and discussion

3.1. Reconstruction calibration, verification and quality assessment

The R27 network clearly captures observed inter-annual temperature variations in the HadCRUT3v Australasian spatial mean (Figure 2, see also section S7). The full R27 network ensemble mean was significantly correlated (r= 0.83) with the instrumental target over the 1921–1990 period; explaining 69% of inter-annual variance in the calibration/verification interval. The reconstruction and instrumental series were then linearly detrended to remove biases associated with the 20th century warming trend. This returned a correlation coefficient of r= 0.67 over the 1921–1990 period (46% of explained inter-annual variance), indicating considerable skill in reproducing inter-annual temperature variations, and the marked influence of global warming in Australasia over recent decades.

The advantage of using an ensemble PCR reconstruction method is shown in Figure 3. Since the reconstruction parameters are varied for each ensemble member, more extensive estimates of reconstruction uncertainty are possible than results based on a single early/late calibration/verification techniques used routinely in palaeoclimatology (for further discussion see Gallant and Gergis, 2011; Gergis *et al.*, 2012). The ensemble mean is considered our 'best estimate' reconstruction (Figure 4) and the solid line indicates years when each of the eight reliability metrics were satisfied, providing a stringent measure of the most 'robust' sections of the reconstruction.

Since the motivation for using the ensemble approach is to perturb the reconstruction parameters to generate extreme uncertainty cases, the ensemble mean reconstruction (Figure 4) is likely to be conservative in comparison with previous reconstructions that tend to provide more limited uncertainty estimation based on single period calibration/verification techniques. As such the thin line represents periods of reduced reliability, but in fact yields a minimum of five out of eight fulfilled reliability criteria. As seen in the lower panel of Figure 3 and Table S2.1, the entire reconstruction back to AD 1000 has consistently positive median verification RE and early verification RE values, so would traditionally be considered a statistically 'skilful' reconstruction (Cook and Kairiukstis, 1990). We conclude that the reconstruction prior to 1430 is skilful but less certain than the sections denoted by the solid line covering periods when more records are available.

The differences between the full R27 proxy network and R21, R14 and R4 subsets are provided in section S2. Note that in the first half of the millennium, uncertainty estimates in the ensemble spread decline when the number of proxies drops below around five records (leaving fewer proxies to include and exclude from the reconstruction), reducing the variability between the ensemble members. This may explain, for example, the comparable uncertainty bands seen around A.D.1100/1500, suggesting more coherence/discrepancies in the reconstruction made up of fewer/more records during these times.

The instrumental verification analyses confirmed that is it possible to reconstruct the September–February (SONDJF) spatial mean of the HadCRUT3v Australasian combined land and ocean temperatures using instrumental data derived from observational data closest to the 27 palaeoclimate records listed in Table 1. The correlation of the SONDJF temperature reconstruction based on these 27 HadCRUT3v grid cells and the full HadCRUT3v predictand was highly significant (r=0.88) over the calibration interval (Figure S3.1), and remained strong even after linear detrending (r=0.75). A mean verification RE of 0.58 was obtained over the 1921–2000 period. Given the data quality issues noted above, it is unsurprising that the reconstruction results are somewhat weaker using the 27 nearest GHCN stations (r=0.73) over the 1953–1992 period (r=0.67 detrended). Once again, a positive mean verification RE of 0.09 was found over the full reconstruction interval (with a positive bias observed in the full histogram of REs provided in Figure S3.2), suggesting that a skilful reconstruction of the HadCRUT3v Australasian SONDJF spatial mean is indeed possible using the R27 network.

A final test of the ability of the reconstruction method to extract a real climate ‘signal’ from noisy proxy data was performed using ten white noise degraded HadCRUT3v instrumental data sets (previously described as ‘pseudo instrumental’ proxies in Section 2.3). An ensemble of reconstructions was generated from each set of pseudo instrumental proxies and the resulting mean reconstruction (Figure S3.3) indicates that skilful reconstructions are possible using these noise degraded data sets. The correlations between the mean reconstructions from the ten sets of pseudo instrumental proxies and the instrumental predictand were statistically significant, ranging from 0.55 to 0.75. The degraded instrumental verification RE values vary and range between -0.26 and 0.09 (Figure S3.3). The results provide evidence that our method can successfully extract an underlying common temperature signal even when it is compounded by extraneous noise.

3.2. Australasian SONDJF temperature variations AD 1000–2001

Having verified the skill of the inter-annual Australasian SONDJF temperature reconstruction, we now examine the full R27 3000-member ensemble to identify decadal scale temperature variations over the past millennium. The results presented here concentrate on periods with large anomalies. Any comparisons between the magnitudes of these anomalies must be internally consistent for each reconstruction to preserve their internal and systematic variability. So, the variations in member-*n* are compared only to member-*n* and these differences are then compared across the entire ensemble. While systematic errors may influence the reconstructed temperature variations within a single member these errors cancel across the ensemble, evidenced by the normal distribution of errors surrounding the mean reconstruction (not shown).

Note that while this discussion focuses on the full R27 network, results for different proxy networks are also presented in Tables 2 and Figures S2.1–S2.3 for comparison. A prominent feature of the reconstruction is the warming beginning around 1900, with the most rapid increase from 1950 (Figure 4). For the R27 ensemble mean, the hottest decade, 30-year and 50-year period occur after 1950. This holds true for 86.2%, 98.3% and 94.5% of individual ensemble members, respectively (see Table S3.1 and Figure S3.4). For the mean reconstruction, the three warmest non-overlapping decades occur consecutively from 1970–1979, 1980–1989 and 1990–1999. It is worth noting that the 2000–2009 decade not covered by the palaeoclimate reconstruction is the warmest recorded in the observational temperature data. Outside of the late 20th century, the next warmest decades in our temperature reconstruction occur during the 1240s and 1330s (Table 2).

There is a warm peak in the mean reconstruction during the 1330s, followed by a cooling trend culminating in the cold interval centred on the 1520s (Figure 4). A relative recovery from cool conditions occurs by the 1580s, before cooling again from 1650–1680. Following brief warm periods centred on 1710 and 1800, a rapid decline in temperature occurs from 1810 until 1860 – the coldest interval in the 1002-year reconstruction. Temperature anomalies during the temperature minimum in 1830–1859 were 0.44^{o}C (±0.18°C) below the 1961–1990 average. Warming starts from the 1860s onward, when a pronounced temperature increase coincides with a rapid rise in anthropogenic greenhouse gas concentrations (see Figure S4.2). The increase in temperature is interrupted by cool intervals ~1900–1910 and again around 1930, before monotonic warming on decadal and longer timescales continues from 1950 to present.

The R27 ensemble mean shows no other warm periods in the past millennium that match or exceed the post-1950 warming observed in the Australasian region. Periods of monotonic warming were determined for individual ensemble members. The longest period of warming across consecutive decades was calculated for each reconstruction. For 92.4% of members, this occurred during the 20th century and for these members almost always included the period from 1950–1999. This conclusion is robust against the proxy network chosen suggesting that highly anomalous late 20th century warming in the region is a robust feature of the reconstruction (Table 2).

3.3. Comparison with solar forcing

The five key solar grand minima based on solar observations over the past millennium are the Oort (1040–1080), Wolf (1280–1350), Spörer (1460–1550), Maunder (1645–1715), and Dalton (1790–1820) low solar periods (Steinhilber and Beer, 2011) (Figure 5). All of these episodes correspond to notable declines in reconstructed temperatures around the 1060s, 1280s, 1320s, 1520s, 1650s, 1680s and 1810s. The Wolf and Spörer intervals, however, also contain periods of relative warmth so do not appear to be exclusively associated with persistent cool temperatures.

Aside from the 1830s (a period coincident with marked internal variations described below), many of the coolest intervals recorded in our reconstruction coincide with solar minima. Average 30-year filtered temperature anomalies during the solar minima are significantly lower than outside the solar minima in the pre-industrial period (A.D. 1000–1850) in 74% of the ensemble members (Figure S8.1). The magnitude of the temperature anomalies observed within and outside of solar minima, however, are relatively minor with an average of 0.03°C (±0.05°C) compared to the 30-year filtered temperature standard deviation A.D. 1000–1850 (0.11±0.03°C). These results suggest the subdued role of solar forcing on regional temperature variations over the past millennium.

The so-called 'Little Ice Age' (LIA) described from the Northern Hemisphere is thought to extend from approximately A.D. 1400–1700, but possibly ending as late as 1850 (Mann *et al.*, 2009; Graham *et al.*, 2011). From the reconstruction presented here, the LIA appears to have a signature in Australasian temperatures from ~A.D. 1500–1840. The coolest 30-year average temperature anomaly reconstructed between 1830–1859 was 0.44^{o}C (±0.18) below the 1961–1990 average.

Between the Oort and Wolf minima, a period of high solar activity from A.D. 1090–1270, coincides with the 'Medieval Climate Anomaly' (MCA), a prolonged warm period identified in many regions of the Northern Hemisphere spanning A.D. 900–1250 (Lamb, 1965; Hughes and Diaz, 1994; Mann et al., 2009; Diaz et al., 2011; Graham et al., 2011). In our Australasian temperature reconstruction, peak medieval warmth is observed around A.D. 1240–1360 (Figure 5). This is somewhat later than described from Northern Hemisphere regions and overlaps with part of the Wolf solar minimum. The average temperature anomaly in the Australian region calculated over the warmest pre-industrial 30-year average A.D. 1238–1267 period is 0.09^{o}C (±0.19°C) below the 1961–1990 climatology.

In general, although many cool events in our reconstruction overlap with solar minima and vice versa, there are also periods where solar forcing does not match Australasian temperature fluctuations, indicating that no consistent decadal-scale response to solar variability in the region during the last millennium. This is reflected in the low correlations of our reconstruction with solar forcing (Steinhilber *et al.*, 2009): 200-year running correlations are significant for more than 50% (25%) of the ensemble members during only 6% (12%) of our reconstruction period (Figure S8.2).

3.4. Comparison with volcanic forcing

The last 1000 years contain a number of volcanic eruptions that correspond to declines in reconstructed Australasian warm season temperatures (Figure 5). During the LIA, several strong volcanic eruptions occurred during solar grand minima, enhancing (regional) cooling. The best examples of this are found in the early 19th century, a period of enhanced tropical volcanism, which includes the Tambora eruption of 1815 and the Dalton solar minimum (Robertson *et al.*, 2001; Gao *et al.*, 2008; D'Arrigo *et al.*, 2009). Although some the largest volcanic eruptions of the last millennium are associated with slightly lagged cold peaks of decadal-scale temperatures (e.g. the 13th-century, 1452 and early 19th century eruptions), there is no significant immediate response to volcanic events identifiable at inter-annual timescales (Figures S8.3–S8.6). From the results presented here, the volcanic signal seems to be weaker in Australasia compared with regional reconstructions from the Northern Hemisphere (Hegerl *et al.*, 2011).

Intriguingly, arguably the largest volcanic event of the past millennium, the A.D. 1258 unknown tropical eruption, does not have a pronounced effect on our reconstructed Australasian temperature reconstruction. Discrepancies between volcanic forcing and reconstructed temperatures are also likely to reflect the fact that internal atmosphere–ocean circulation is the dominant source of variability on continental/regional scales, rather than external forcing which has been demonstrated to be more important on hemispheric/global scales (Goosse *et al.*, 2005).

3.5. Climate model comparison

From the start of industrialisation around 1850, the influence of solar and volcanic forcing on global climate begins to be overwhelmed by the rapid increase in anthropogenic greenhouse gas concentrations (Hegerl *et al.*, 2007a; Hegerl *et al.*, 2007b; Jansen *et al.*, 2007). Figure 6 shows reconstructed Australasian SONDJF temperatures and the ensemble mean of three transient CSIRO Mk3L model simulations relative to the 1961–1990 reference period to match the reconstruction. While the reconstruction and model simulations align well during the post 1850 industrial era, and reasonably well during some periods of volcanic eruptions, the model is generally too cool during the pre-industrial era. This cool bias suggests that the sensitivity of the model to anthropogenic greenhouse gases is a little too high relative to the reconstruction. Alternatively, this may reflect the fact that the model simulations omit the effects of several anthropogenic forcings, particularly changes in tropospheric aerosols, stratospheric ozone, vegetation and land use over the 1961–1990 base period. This may cause temperature anomalies to be too warm in recent decades (due to the absence of anthropogenic aerosol emissions, especially sulphates, that moderate the rate of warming due to anthropogenic greenhouse gases) and subsequently overestimate temperature anomalies in past centuries. A possible loss of low frequency variance in the reconstruction (e.g. Esper *et al.*, 2005) may also explain parts of the lower amplitude in the reconstruction compared to the climate model simulations.

Using a three-member model ensemble allows us to better estimate decadal variability due to internal noise from forced responses seen in the ensemble mean of the model simulations. While the correlation between the 30-year filtered temperature reconstruction and model ensemble mean over the full A.D. 1000–2000 period is significant ($r=0.33$, $p<0.05$), the discrepancies noted above are clear, particularly in the pre-1300 section of the reconstruction (Table 3). Given that the amplitude and timing of specific unforced variations cannot be reproduced in model simulations because of their stochastic nature, the reconstructed inter-decadal variations in the pre-industrial period match the model simulations quite well (see Table 3 and section S4).

For example, Figure 6 shows that while some of the temperature declines in the reconstruction are coincident with major volcanic events over the past millennium (particularly Kuwae in 1452 and Tambora in 1815), they do not coincide with all the temperature declines associated with volcanic forcing in the model. Reasons for this may be because the volcanic forcing dataset is exaggerating the magnitude of these eruptions (Robock, 2000) or the loss of variance associated with palaeoclimate reconstructions (Esper *et al.*, 2005).

When shown relative to a 'pre-industrial baseline' of A.D. 1500–1850 (Figure S4.1), there are only two pre-1900 periods in the mid-11th century and mid-13th century when the model ensemble mean exceeds the reconstruction's uncertainty estimates. The latter is likely to be a direct result of the A.D. 1258 volcanic forcing. Despite widespread evidence of a major volcanic eruption and climatic impacts (Stothers, 2000; Oppenheimer, 2003), Figure 6 shows that this event does not appear to be significant in the Australasian region. Conversely, the mid-11th century modelled temperature anomaly may reflect inadequacies in regional volcanic and solar forcing data. This period coincides with the Oort solar minimum but the timing and amplitude of solar variations are substantially more uncertain during the first half of the millennium (Hegerl *et al.*, 2007a). Once again, these issues may reflect the fact that internal atmosphere–ocean forcing is the dominant source of variability on regional/continental scales (Goosse *et al.*, 2005).

The relative roles of forced and unforced climate variability and change were also examined using the climate model simulations (Phipps *et al.*, 2012). Figure S4.2 shows the evolution of the Australasian mean SONDJF temperature over the last millennium, according to both the three forced simulations and three representative 1000-year sections of the unforced control simulation. On decadal timescales, differences between the ensemble members reveal stochastic variability arising from internal dynamics of the coupled atmosphere–ocean system. However, a common signal across the model ensemble mean also reveals the forced response to the three largest volcanic eruptions of the last millennium (AD 1258, Kuwae and Tambora).

On multi-decadal timescales, forced changes dominate over unforced internal variability in the model. However, in the reconstruction, the largest known volcanic eruption occurs during the warmest pre-industrial period (Table 2), while during the coldest period there is no anomalous solar forcing or large volcanic eruptions.

Conversely, in recent decades, anthropogenic forcing has a clear signal in the model data and is consistent with Australasian temperatures on decadal timescales, suggesting it is a possible mechanism for recent increases in Australasian temperatures (e.g. Karoly and Braganza, 2005). To assess the probability of the late 20th century warming occurring by chance due to unforced natural climate variability, we examined a 10,000-year pre-industrial control simulation using the CSIRO Mk3L climate system model.

Figure 7 shows the distribution of the changes in the mean Australasian SONDJF temperature between consecutive 50-year periods of this simulation. Over the full 10,000 years, the difference in temperature between consecutive 50-year periods never exceeds 0.10^{o}C in magnitude. This contrasts with the reconstructed and measured (inter-annual) ensemble mean temperature change of 0.32^{o}C ±0.06^{o}C between 1901–1950 and 1951–2000. Figures S4.2, S4.3 and Section S8 provide further evidence that the post 1950 warming cannot be explained by natural factors alone. Figure

8.2 shows that the rapid rise in greenhouse gas concentrations observed in the late 20th century is the dominant driver of temperature changes over recent decades. Thus, in the CSIRO Mk3L model, anthropogenic forcing is required to produce the post 1950 warming observed in the reconstruction. This suggests that the post 1950 warming did not arise as a result of unforced natural variability of the coupled atmosphere–ocean system (Figure S4.3).

This result is consistent with detection and attribution studies that clearly attribute the post 1950 temperature increase noted in instrumental global and Australian temperature records to increases atmospheric greenhouse gas concentrations (Karoly and Braganza, 2005; Hegerl *et al.*, 2007a). The results presented here and in Phipps *et al*. (2012) demonstrate that anthropogenic factors are needed to explain the most anomalous warm period observed in the Australasian region over the past 1000 years. For an extensive data–model comparison and regional attribution study for Australasia over the last 1000 years, the reader is referred to Phipps *et al*. 2012.

4. Comparisons with independent palaeoclimate records

4.1. Temperature flucatuations over the last millennium

Peak pre-industrial warmth in Australasian temperature is observed around A.D. 1240–1360, somewhat later than warming described from Northern Hemisphere regions (Figure 4). From the ensemble mean ‘best estimate’ presented here, the average temperature anomaly in the Australian region for the 1238–1267 period is 0.09^{o}C (±0.19°C) below 1961–1990 levels. This 30-year temperature anomaly is comparable with Northern Hemisphere results that suggest that maximum pre-industrial temperatures were probably between 0.1–0.2^{o}C below the 1961–1990 mean and significantly below warm anomalies observed in instrumental records after 1980 (Jansen *et al.*, 2007). Reconstructed SSTs from a sedimentary record from the Makassar Strait (3^{o}S, 119^{o}E) provides independent support for large positive anomalies similar to, though not significantly warmer than modern values between ~A.D. 1000–1400 (Newton *et al.*, 2006; Oppo *et al.*, 2009).

The shift from peak pre-industrial warmth into a pronounced cooling ~A.D. 1300–1400 is supported by palaeoclimate evidence and archaeological interpretations that indicate significant societal impacts across the Pacific Basin at this time (Nunn, 2000; Nunn, 2007). The high-resolution temperature reconstruction presented in Figure 4 suggests that a transition to cooler conditions in the Australasian region is likely to have occurred after ~A.D. 1330. This timing agrees with a shift in low frequency (centennial) circulation features in a reconstruction of mean synoptic flow patterns for New Zealand that implicates enhanced westerly flow between ~A.D. 1250–1360 . There is evidence that a more 'zonal' regime is associated with a shift from warm to cool climate conditions, with cooler conditions associated with intensified atmospheric blocking in the southwest Pacific during this period (Lorrey *et al.*, 2008; Lorrey *et al.*, 2011).

The results presented in Section 3 indicate that from the early 1300s onward, there is a gradual cooling into a period that coincides with the timing of the Little Ice Age (LIA) interval, described from the Northern Hemisphere as occurring between A.D. 1400–1700 (Mann *et al.*, 2009), or more generally from A.D. 1500 to as recently as the beginning of the industrial era around 1850 (Mann *et al.*, 2009; Graham *et al.*, 2011). Figure 4 suggests that similar cooling in the Australasian region may have occurred somewhat earlier than the LIA period traditionally defined from the Northern Hemisphere. Since our reconstruction may not be as spatially representative of the full Australasian region at this time, it may mostly reflect variations experienced in the extra-tropical region of our domain (see Table 1). Nonetheless section S2, which compares the earliest reconstruction nest with the full ensemble mean reconstruction, shows that aside from a loss of variance, the R4 network still adequately represents the broader Australasian region. Independent evidence for a coherent Southern Hemisphere cool period from as early 1300s is also seen from low resolution tropical Indonesian marine sediments (Oppo *et al.*, 2009).

Using a network of cave records and other hydroclimatic proxies, Lorrey *et al.* (2008) suggest the general dominance of circulation patterns in the New Zealand sector that are associated with cooler temperatures for the latter half of the last millennium until the late 19th century. An independent coral composite record from the Great Barrier Reef, Australia indicate that from A.D. 1565 to 1700 SSTs off northeastern Australia were 0.2°–0.3°C cooler and more saline than 1860–

1985 averages (Hendy *et al.*, 2002). This cooling is in general agreement with a high-resolution sedimentary record from Indonesia that suggests between 1550–1850, SSTs were 0.5°–1°C colder than modern values (Oppo *et al.*, 2009).

The 1700–1850 period is recognised from Antarctica as being one of the most abrupt climate shifts of the last 1000 years (Goodwin *et al.*, 2004; Mayewski *et al.*, 2004; Mayewski *et al.*, 2009). During this time, ice cores indicate an increase in sea ice extent and an intensification of the westerly winds in the mid-high latitudes of the Southern Hemisphere (Goodwin *et al.*, 2004; Mayewski *et al.*, 2004), characteristic of a positive Southern Annular Mode (SAM) phase. Comparable conditions to this early 19th century event are thought to have occurred during the A.D. 1886–1903 and 1920–1929 periods (Goodwin *et al.*, 2004), also associated with cooling in our reconstruction.

Finally, the idea of Australasia-wide cooling from the middle of the last millennium to the 19th century is further supported by evidence of glacier fluctuations from New Zealand's Southern Alps (~43^{o}S, 170^{o}E). The timing of major ice advances centred on 1605±70, 1735±50, 1785±10 and1845±40 (Schaefer *et al.*, 2009) suggests that pronounced cooling also influenced the Southern Hemisphere region of Australasia particularly from the mid 16th–mid 19th century.

4.2. Ocean–atmosphere interactions

While low frequency variations of internal ocean–atmosphere interactions like the El Niño–Southern Oscillation (ENSO) are known to have played an important role in influencing regional temperature variations over the past millennium (Mann *et al.*, 2005; Hegerl *et al.*, 2007a; Mann *et al.*, 2009; Li *et al.*, 2011), the nature and stability of regional climate variations are still unclear (Lough, 2011; Gergis *et al.*, 2012). To assess the relationship of reconstructed Australasian warm season temperatures and ENSO teleconnection, we compared our R27 reconstruction with the Unified ENSO Proxy (UEP) developed by McGregor *et al*. (2010). The UEP represents the first uncalibrated EOF of ten published ENSO reconstructions back to A.D. 1650 and probably represents the least spatially-biased ENSO reconstruction currently available. Since a number of the palaeoclimate records used in the current study have also been used in our previous ENSO reconstruction work (Braganza *et al.*, 2009), the UEP was recalculated removing the Braganza *et al*. (2009) data (proxies three and nine in McGregor *et al*. (2010)) to provide independent comparison with our Australasian temperature reconstruction.

The relationship between inter-annual and inter-decadal ENSO variability and Australian temperature is known to fluctuate over the 20th (Power *et al.*, 1999; Jones and Trewin, 2000). The correlation coefficient between the 30-year filtered versions of the SOI (UEP) and our HadCRUT3v SONDJF temperature predictand over the instrumental period is r= -0.34 (r= -0.32). Figure 8 shows the 30-year running correlation between our inter-annual Australasian SONDJF temperature reconstruction and the UEP in the post-1649 interval of overlap. The results display a mostly negative relationship over the full period (r= -0.49) with considerable variability over past centuries. Figure 7 confirms notable fluctuations in the influence of Pacific Ocean driven climate variability and temperatures in the Australasian region during the instrumental period (e.g. the 1930s and 1940s), and lesser-known instabilities seen in the early 18th and 19th centuries.

Graham *et al*. (2011) present results from a coupled GCM showing that a slight warming of the tropical Indian and western Pacific Oceans relative to the other tropical ocean basins may have induced a broad range of the circulation and climate changes indicated by proxy data in the medieval period, including many of those not explained by a cooler eastern tropical Pacific alone. They suggest that tropical SSTs were the principal driver of large-scale climate variations during the MCA, which was characterised by an enhanced zonal Indo-Pacific SST gradient. However, if the Indo Pacific Warm Pool was indeed the origin of the relative warmth associated with the MCA, then the temperature signal would be expected to be stronger in the Australasian region than in hemispheric means. The lack of any strong ‘MCA signal’ in the reconstruction presented here therefore appears to be inconsistent with the Graham *et al*. (2011) hypothesis, or may reflect inadequacies in availability of records from tropical regions of Australasia during this period.

Shifts in ENSO variability in the core dynamical region of the Indo–Pacific region may correspond to notable period of warmth reported in the high latitude region of the Southern Ocean. Goosse *et al*. (2004) have proposed a delayed response to natural forcing due to the storage and transport of heat anomalies by the deep ocean to explain the warm Southern Ocean around 1300s to 1400s as inferred from three Southern Hemisphere climate proxies used by Mann and Jones (2003) and additional Antarctic ice cores.

The delay in the Southern Hemisphere temperature response to external climate forcing may have implications for the evolution of future climate change in the region. Model studies suggest that the present-day Southern Ocean temperatures lag the increases in greenhouse-gas concentrations observed during the recent decades (Goosse *et al.*, 2004). This implies that it is possible that large warming of the Southern Ocean will occur when the warm deep water formed during the 20th century reaches the surface in coming decades (Goosse *et al.*, 2004).

4.3. Comparison with Australian borehole temperature reconstruction

A comparison with the only continental-scale Australian borehole temperature reconstruction available for IPCC AR4 indicates that the (low frequency) borehole estimates fall within the cooler section of our uncertainty estimates until around 1800, before shifting closer to our ‘best estimate’ ensemble mean or the warmer uncertainty range until present day (Figure S5). This confirms the expected result that the rise in surface temperatures over the Australian landmass has been greater than within a broader regional domain combining land and ocean temperatures.

Since most of the boreholes were logged prior to 1976, the observed subsurface temperatures do not capture the strong warming experienced by Australia in the last two decades of the 20th century (Pollack *et al.*, 2006), but is captured in the temperature reconstruction presented here. In terms of cold periods, the borehole record suggests that the 17th century was the coolest interval, in contrast to the strong evidence for coldest conditions in the Australasian region between 1810–1860. This highlights the inability of boreholes used in IPCC AR4 (Pollack *et al.*, 2006; Jansen *et al.*, 2007) to adequately capture the multi-decadal variations seen in Figure 4, and the importance of high-resolution palaeoclimatology in improving estimates of regional decadal climate variations.

Overall, the results presented here suggest that the second half of the 20th century (1951–2000) was 0.34°C warmer than average preindustrial conditions (A.D. 1651–1700, the cold phase before the borehole temperatures start to increase). This corresponds with the Australian (land-only) borehole estimate and the Northern Hemisphere (Mann *et al.*, 2008) of 0.52°C and 0.56°C, respectively. The differences in magnitude between these anomalies may reflect the small land/sea ratio for the Australasian region, perhaps combined with a delayed Southern Hemisphere response to anthropogenic warming.

5. Conclusions

This study presents the first warm season (September–February) temperature reconstruction for the Southern Hemisphere combined land and oceanic region of Australasia. To provide robust uncertainty estimates, we perform an ensemble Principal Component Reconstruction (PCR) technique using 27 temperature proxies from the region. The R27 (R4) proxy network was significantly correlated (r= 0.83 (0.67)) with the HadCRUT3v SONDJF spatial mean temperature over the 1921–1990 period. Application of eight stringent reconstruction reliability metrics identified the period after A.D. 1430 as the highest quality section of the reconstruction, but also revealed a skilful reconstruction is possible over the entire millennium.

There is broad agreement between reconstructed and CSIRO Mk3L model simulated temperatures during the pre-industrial era. Solar and volcanic forcing does not seem to have a distinct and consistent signal in the reconstructed decadal-scale temperature variations and appear to be masked by internal variability. In contrast, the response of Australasian temperature variations to anthropogenic forcing is clear. The results presented here and in Phipps *et al*. (2012) demonstrate that anthropogenic factors are needed to explain the most anomalous warm period reconstructed in the Australasian region over the past 1000 years. This finding is consistent with detection and attribution studies that clearly attribute the post 1950 temperature increase noted in instrumental global and Australian temperature records to increases atmospheric greenhouse gas concentrations (Karoly and Braganza, 2005; Hegerl *et al.*, 2007a).

Our reconstruction suggests that peak pre-industrial warmth occurred in Australasia around A.D. 1240–1360, somewhat later than described from Northern Hemisphere regions. The maximum temperature anomaly in the Australian region calculated over the A.D. 1238–1267 period is 0.09^{o}C (±0.19°C) below 1961–1990 levels. It is worth noting that this medieval warming occurred in the absence of significant anthropogenic greenhouse gas emissions, thus is not analogous to post 1950 observed warming which is predominantly anthropogenically-forced (Karoly and Braganza, 2005; Hegerl *et al.*, 2007a). This implies that if the full range of natural climate variability has not yet been observed in Australasia, anthropogenic forcing may led to future ‘climate surprises’ that may manifest, for example, as changes in the frequency and duration of regional temperature extremes (Alexander and Arblaster, 2009).

Following maximum pre-industrial warmth around A.D.1330, a cooling trend that lasts several hundred years begins. This cooling eventuates in a minimum temperature anomaly of -0.44^{o}C by ~1840 during the peak of the Northern Hemisphere’s ‘Little Ice Age’. Our results support the notion that a pronounced cool period consistent with the timing of the LIA extended well outside of the Northern Hemisphere high latitudes and into the tropical and subtropical regions of the Southern Hemisphere (Newton *et al.*, 2006).

The results introduced here are significant for a number of reasons. This Australasian temperature reconstruction is the first high-resolution, multi-proxy study available for the region, and only the second large-scale regional synthesis available from the Southern Hemisphere (Neukom *et al.*, 2011). Given that instrumental observations in Australasia generally extend back, at best, to the early 20th century, the palaeoclimate temperature estimates presented here now provide an extended basis for evaluating the accuracy of climate models in simulating past regional climate variability and an opportunity to reduce uncertainties associated with future climate variability and change (Hegerl et al., 2006; Hegerl et al., 2011). This study provides pre-industrial estimates of decadal temperature variations as far back as A.D. 1000, which may help to quantify the role of natural and anthropogenic forcing on regional climate variations as demonstrated in other regions of the world (Hegerl *et al.*, 2006; Hegerl *et al.*, 2011).

Our work provides a significant improvement on the uncertainties reported in the IPCC AR5 for the Australasian region (CSIRO, 2007; Jansen *et al.*, 2007), and Northern Hemisphere-centric understanding of climate variations that have occurred over the past 1000 years (Lamb, 1965; Grove, 1988; Hughes and Diaz, 1994; Crowley and Lowery, 2000; Bradley *et al.*, 2003; Mann *et al.*, 2009; Graham *et al.*, 2011). Future research will focus on consolidating Australasian palaeoclimate data with other Southern Hemisphere regions to advance our understanding of global change over the past millennium.

6. Acknowledgments

We are grateful to all Aus2K working group members for data contributions and helpful discussions that clarified the study. Ed Cook is thanked for providing access to the signal-free tree ring standardisation program and Shayne McGregor is acknowledged for use of the modified version of the Unified ENSO Proxy used in this analysis. We acknowledge funding support from the Australian Department of Energy Efficiency and Environment, the Australian Research Council Projects LP0990151, FF0668679 and DP1092945, and Past Global Changes. SJP acknowledges the NCI National Facility at the Australian National University. We are indebted to all NOAA WDC data contributors who make multi-proxy research possible.

7. References

Alexander, L. and J. Arblaster, 2009: Assessing trends in observed and modelled climate extremes over Australia in relation to future projections. *International Journal of Climatology*, **29**, 417–435.

Allen, K. J., E. Cook, R. Francey and K. Michael, 2001: The climatic response of *Phyllocladus aspleniifolius* (Labill.) Hook. f in Tasmania. *Journal of Biogeography*, **28**, 305-316.

Bradley, R. S., M. K. Hughes and H. F. Diaz, 2003: Climate in Medieval Time. *Science*, **302**, 404-405.

Braganza, K., J. Gergis, S. Power, J. Risbey and A. Fowler, 2009: A multiproxy index of the El Nino–Southern Oscillation, A.D. 1525–1982. *Journal of Geophysical Research*, **114**, D05106.

Brohan, P., J. Kennedy, I. Harris, S. F. B. Tett and P. D. Jones, 2006: Uncertainty estimates in regional and global observed temperature changes: A new data set from 1850. *Journal of Geophysical Research*, **111**, doi:10.1029/2005JD006548.

Buckley, B., E. Cook, M. Peterson and M. Barbetti, 1997: A changing temperature response with elevation for Lagarostrobis franklinii in Tasmania, Australia. *Climatic Change*, **36**, 4770498.

Chambers, L. E. and G. M. Griffiths, 2008: The changing nature of temperature extremes in Australia and New Zealand. *Australian Meteorological Magazine*, **57**, 13-35.

Charles, C., K. Cobb, M. Moore and R. Fairbanks, 2003: Monsoon–tropical ocean interaction in a network of coral records spanning the 20th century. *Marine Geology*, **201**, 207-222.

Cobb, K., C. Charles, H. Cheng and L. Edwards, 2003: El Nino/Southern Oscillation and tropical Pacific climate during the last millennium. *Nature*, **424**, 271-276.

Cook, E. and L. Kairiukstis, 1990: *Methods of Dendrochronology*. Kluwer Academic Publishers, Cook, E., B. Buckley, R. D'Arrigo and M. Peterson, 2000: Warm-season temperatures since 1600 BC reconstructed from Tasmanian tree rings and their relationship to large-scale sea surface temperature anomalies. *Climate Dynamics*, **16**, 79-91.

Cook, E., J. Palmer, B. Cook, A. Hogg and R. D'Arrigo, 2002a: A multi-millennial palaeoclimatic resource from Lagarostrobos colensoi tree-rings at Oroko Swamp, New Zealand. *Global and Planetary Change*, **33**, 209-220.

Cook, E., J. Palmer and R. D'Arrigo, 2002b: Evidence for a "Medieval Warm Period" in a 1,100 year tree-ring reconstruction of past austral summer temperature in New Zealand. *Geophysical Research Letters*, **29**, 12/1-12/4.

Cook, E., B. Buckely, J. Palmer, P. Fenwick, M. Peterson, G. Boswijk and A. Fowler, 2006: Millennia-long tree-ring records from Tasmania and New Zealand: a basis for modelling climate variability and forcing, past, present and future. *Journal of Quaternary Science,* **21**, 689–699.

Crowley, T. J. and T. S. Lowery, 2000: How Warm Was the Medieval Warm Period? *Ambio*, **29**, 51-54.

CSIRO, 2007: *Climate change in Australia: technical report 2007*. Commonwealth Scientific and Industrial Research Organsiation (CSIRO),

D'Arrigo, R., E. Cook, M. Salinger, J. Palmer, P. Krusic, B. Buckley and R. Villalba, 1998: Tree-ring records from New Zealand: long-term context for recent warming trend. *Climate Dynamics*, **14**, 191-199.

D'Arrigo, R., E. Cook, R. Villalba, B. Buckley, M. Salinger, J. Palmer and K. Allen, 2000: Trans-Tasman Sea Climate Variability Since AD 1740 Inferred From Middle-High Latitude Tree-Ring Data. *Climate Dynamics*, **16**, 603-610.

D'Arrigo, R., R. Wilson and A. Tudhope, 2009: The impact of volcanic forcing on tropical temperatures during the past four centuries. *Nature Geoscience*, **2**, 51–56.

D'Arrigo, R. D., B. M. Buckley, E. R. Cook and W. S. Wagner, 1996: Temperature-sensitive tree-ring width chronologies of pink pine (Halocarpus biformis) from Stewart Island, New Zealand. *Palaeogeography Palaeoclimatology Palaeoecology*, **119**, 293-300.

Della-Marta, P., D. Collins and K. Braganaza, 2004: Updating Australia’s high-quality annual temperature dataset. *Australian Meteorological Magazine*, **53**, 75–93.

Diaz, H. F., R. Trigo, M. K. Hughes, M. E. Mann, E. Xoplaki and D. Barriopedro, 2011: Spatial and Temporal Characteristics of Climate in Medieval Times Revisited. *Bulletin of the American Meteorological Society*, **92**, 1487-1500.

Duncan, R. P., P. Fenwick, J. G. Palmer, M. S. McGlone and C. S. M. Turney, 2010: Non-uniform interhemispheric temperature trends over the past 550 years. *Climate Dynamics*, **35**, 1429-1438.

Ekaykin, A., V. Lipenkov, I. Kuzmina, J. Petit, V. Masson-Delmotte and S. Johnsen, 2004: The changes in isotope composition and accumulation of snow at Vostok station, East Antarctica, over the past 200 years. *Annals of Glaciology*, **39**, 569-575.

Esper, J., D. C. Frank, R. Wilson and K. R. Briffa, 2005: Effect of scaling and regression on reconstructed temperature amplitude for the past millennium. *Geophysical Research Letters*, **32**, doi:10.1029/2004GL021236.

Fowler, A., G. Boswijk, J. Gergis and A. Lorrey, 2008: ENSO history recorded in *Agathis australis* (Kauri) tree-rings Part A: Kauri's potential as an ENSO proxy. *International Journal of Climatology*, **28**, 1-20.

Gallant, A. J. E. and J. Gergis, 2011: An experimental streamflow reconstruction for the River Murray, Australia, 1783–1988. *Water Resources Research*, **47**, doi:10.1029/2010WR009832.

Gao, C., A. Robock and C. Ammann, 2008: Volcanic forcing of climate over the past 1500 years: An improved ice core-based index for climate models. *Journal of Geophysical Research*, **113**, D23111.

Gergis, J., A. J. E. Gallant, K. Braganza, D. J. Karoly, K. Allen, L. Cullen, R. D'Arrigo, I. Goodwin, P. Grierson and S. McGregor, 2012: On the long-term context of the 1997–2009 ‘Big Dry’ in south-eastern Australia: insights from a 206-year multi-proxy rainfall reconstruction *Climatic Change*, **111**, 923–944.

Goodwin, I., T. van Ommen, M. Curran and P. Mayeweski, 2004: Mid latitude winter climate variability in the South Indian and southwest Pacific regions since 1300 AD. *Climate Dynamics*, **22**, 783-794.

Goosse, H., V. Masson-Delmotte, H. Renssen, M. Delmotte, T. Fichefet, V. Morgan, T. van Ommen, B. K. Khim and B. Stenni, 2004: A late medieval warm period in the Southern Ocean as a delayed response to external forcing? *Geophysical Research Letters*, **31**, L06203.

Goosse, H., H. Renssen, A. Timmermann and R. S. Bradley, 2005: Internal and forced climate variability during the last millennium: a model-data comparison using ensemble simulations. *Quaternary Science Reviews*, **24**, 1345-1360.

Graham, N., C. Ammann, D. Fleitmann, K. Cobb and J. Luterbacher, 2011: Support for global climate reorganization during the “Medieval Climate Anomaly”. *Climate Dynamics*, **37**, 1217-1245.

Grove, J. M., 1988: *The Little Ice Age*. Methuen & Co. Ltd,

Hegerl, G., F. Zwiers, P. Braconnot, N. Gillett, Y. Luo, J. Marengo Orsini, N. Nicholls, J. Penner and P. Stott, 2007a: *Understanding and Attributing Climate Change. In: Climate Change 2007: The Physical Science Basis. Contribution of Working Group I to the Fourth Assessment Report of the Intergovernmental Panel on Climate Change*, S. Solomon, D. Qin, M. Manning, Z. Chen, M. Marquis, K. B. Averyt, M. Tignor and H. L. Miller (eds.), Cambridge University Press, Cambridge, United Kingdom and New York, NY, USA.,

Hegerl, G., J. Luterbacher, F. González-Rouco, S. Tett, T. Crowley and E. Xoplaki, 2011: Influence of human and natural forcing on European seasonal temperatures. *Nature Geoscience*, **4**, 99–103.

Hegerl, G. C., T. J. Crowley, W. T. Hyde and D. J. Frame, 2006: Climate sensitivity constrained by temperature reconstructions over the past seven centuries. *Nature*, **440**, 1029-1032.

Hegerl, G. C., T. J. Crowley, M. Allen, W. T. Hyde, H. N. Pollack, J. Smerdon and E. Zorita, 2007b: Detection of human influence on a new, validated 1500-year temperature reconstruction. *Journal of Climate*, **20**, 650-666.

Hendy, E., M. Gagan, C. Alibert, M. Mc Culloch, J. Lough and P. Isdale, 2002: Abrupt Decrease in Tropical Pacific Sea Surface Salinity at End of Little Ice Age. *Science*, **295**, 1511-1514.

Hennessy, K., B. Fitzharris, B. Bates, N. Harvey, S. Howden, L. Hughes, J. Salinger and R. Warrick, 2007: *Australia and New Zealand.* , Cambridge University Press,, 507-540.

Huang, S., H. Pollack and P. Y. Shen, 2000: Temperature trends over the past five centuries reconstructed from borehole temperatures. *Nature*, **403**, 756-758.

Hughes, M. and H. Diaz, 1994: Was there a “Medieval Warm Period” and if so, where and when? *Climatic Change*, **26**, 109–142.

Jansen, E., J. Overpeck, K. Briffa, J. Duplessy, F. Joos, V. Masson-Delmotte, D. Olago, B. Otto-Bliesner, W. Peltier, S. Rahmstorf, R. Ramesh, D. Raynaud, D. Rind, O. Solomina, R. Villalba and D. Zhang, 2007: *Palaeoclimate,* S. Solomon, D. Qin, M. Manning, Z. Chen, M. Marquis, K.B. Averyt, M. Tignor and H.L. Miller (eds.), Cambridge University Press, 433-497.

Jones, D. and B. Trewin, 2000: On the relationship between the El Nino-Southern Oscillation and Australian land surface temperature. *International Journal of Climatology,* **20**, 697–719.

Jones, P., K. Briffa, T. Barnett and S. Tett, 1998: High-resolution Palaeoclimatic Records for the last Millennium: Interpretation, Integration and Comparison with General Circulation Model Control-run Temperatures. *The Holocene*, **8**, 455-471.

Jones, P. and M. Mann, 2004: Climate over past millennia. *Reviews of Geophysics*, **42**, 1-42.

Jones, P., K. Briffa, T. Osborn, J. Lough, T. van Ommen, B. Vinther, J. Luterbacher, E. Wahl, F. Zwiers, M. Mann, G. Schmidt, C. Ammann, B. Buckley, K. Cobb, J. Esper, H. Goose, N.

Graham, E. Jansen, T. Kiefer, C. Kull, M. Kuttel, E. Mosley-Thompson, J. Overpeck, N. Riedwyl, M. Schulz, A. Tudhope, R. Villalba, H. Wanner, E. Wolff and E. Xoplaki, 2009: High-resolution palaeoclimatology of the last millennium: a review of current status and future prospects. *The Holocene*, **19**, 3-49.

Jones, P. D., M. New, D. E. Parker, S. Martin and I. G. Rigor, 1999: Surface air temperature and its changes over the past 150 years. *Review of Geophysics*, **37**, 173-199.

Karoly, D. J. and K. Braganza, 2005: Attribution of Recent Temperature Changes in the Australian Region. *Journal of Climate*, **18**, 457-464.

Keenan, T. D. and H. A. Cleugh, 2011: Climate Science Update: A Report to the 2011 Garnaut Review. Centre for Australian Weather and Climate Research (CAWCR) Technical Report No. 036

Kuhnert, H., J. Patzold, B. Hatcher, K. Wyrwoll, A. Eisenhauer, L. Collins, Z. Zhu and G. Wefer, 1999: A 200-year coral stable oxygen isotope record from a high-latitude reef off Western Australia. *Coral Reefs*, **18**, 1-12.

Kuhnert, H., J. Pätzold, K. Wyrwoll and G. Wefer, 2000: Monitoring climate variability over the past 116 years in coral oxygen isotopes from Ningaloo Reef, Western Australia. *International Journal of Earth Sciences*, **88**, 725–732.

Lamb, H. H., 1965: The early medieval warm epoch and its sequel. *Palaeogeography, Palaeoclimatology, Palaeoecology*, **1**, 13-37.

Li, J., S. P. Xie, E. R. Cook, G. Huang, R. D'Arrigo, F. Liu, J. Ma and X. T. Zheng, 2011: Interdecadal modulation of El Nino amplitude during the past millennium. *Nature Climate Change*, **1**, 114–118

Linsley, B., G. Wellington, D. Schrag, L. Ren, J. Salinger and A. Tudhope, 2004: Geochemical evidence from corals for changes in the amplitude and spatial pattern of South Pacific interdecadal climate variability over the last 300 years. *Climate Dynamics*, **22**, 1-11.

Linsley, B., P. Zhang, A. Kaplan, S. Howe and G. Wellington, 2008: Interdecadal-decadal climate variability from multicoral oxygen isotope records in the South Pacific Convergence Zone region since 1650 A.D. *Paleoceanography*, **23**, 1-16.

Linsley, B. K., A. Kaplan, Y. Gouriou, J. Salinger, P. B. Demenocal, G. M. Wellington and S. S. Howe, 2006: Tracking the extent of the South Pacific Convergence Zone since the early 1600s. *Geochemistry Geophysics Geosystems*, **7**, doi:10.1029/2005GC001115.

Lorrey, A., P. Williams, J. Salinger, T. Martin, J. Palmer, A. Fowler, J. Zhao and H. Nail, 2008: Speleothem stable isotope records interpreted within a multi-proxy framework and implications for New Zealand palaeoclimate reconstruction. *Quaternary International*, **187**, 52-75.

Lorrey, A., I. Goodwin, J. Renwick and S. Browning, 2011: Blocking circulation anomalies in the Tasman Sea region during the Medieval Climate Anomaly. *PAGES News*, **19**, 22–23.

Lough, J. M., 2011: Great Barrier Reef coral luminescence reveals rainfall variability over northeastern Australia since the 17th century. *Paleoceanography*, **26**, doi:10.1029/2010PA002050.

Lough, J. M. and A. J. Hobday, 2011: Observed climate change in Australian marine and freshwater environments. *Marine and Freshwater Research*, **62**, 984-999.

Luterbacher, J., E. Xoplaki, D. Dietrich, R. Rickli, J. Jacobeit, C. Beck, Gyalistras, C. Schmutz and H. Wanner, 2002: Reconstruction of sea level pressure fields over the Eastern North Atlantic and Europe back to 1500. *Climate Dynamics*, **18**, 545-561.

MacFarling–Meure, C., D. Etheridge, C. Trudinger, P. Steele, R. Langenfelds, T. van Ommen, A. Smith and J. Elkins, 2006: Law Dome CO2, CH4 and N2O ice core records extended to 2000 years BP. *Geophysical Research Letters*, **33**, doi:10.1029/2006GL026152.

Mann, M. and P. Jones, 2003: Global surface temperatures over the past two millennia. *Geophysical Research Letters*, **30**, doi:10.1029/2003GL017814.

Mann, M., M. Cane, S. Zebiak and A. Clement, 2005: Volcanic and Solar Forcing of the Tropical Pacific over the Past 1000 Years. *Journal of Climate*, **18**, 447-456.

Mann, M., Z. Zhang, M. Hughes, R. Bradley, S. Miller, S. Rutherford and F. NI, 2008: Proxy-based reconstructions of hemispheric and global surface temperature variations over the past two millennia. *Proceedings of the National Academy of Sciences*, **105**, 13252–13257.

Mann, M., Z. Zhang, S. Rutherford, R. Bradley, M. Hughes, D. Shindell, C. Ammann, G. Faluvegi and F. Ni, 2009: Global signatures and dynamical origins of the Little Ice Age and Medieval Climate Anomaly. *Science*, **326**, 1256–1260.

Mayewski, P. A., K. A. Maasch, J. W. C. White, E. J. Steig, E. Meyerson, I. Goodwin, V. I. Morgan, T. Van Ommen, M. A. J. Curran, J. Souney and K. Kreutz, 2004: A 700 year record of Southern Hemisphere extratropical climate variability. *Annals of Glaciology*, **39**, 127-132.

Mayewski, P. A., M. P. Meredith, C. P. Summerhayes, J. Turner, A. Worby, P. J. Barrett, G. Casassa, N. A. N. Bertler, T. Bracegirdle, A. C. Naveira Garabato, D. Bromwich, H. Campbell, G. S. Hamilton, W. B. Lyons, K. A. Maasch, S. Aoki, C. Xiao and T. van Ommen, 2009: State of the Antarctic and Southern Ocean climate system. *Rev. Geophys.*, **47**, RG1003.

McGregor, S., A. Timmermann and O. Timm, 2010: A unified proxy for ENSO and PDO variability since 1650. *Climate of the Past*, **6**, 1–17.

McShane, B. and A. Wyner, 2011: A Statistical Analysis of Multiple Temperature Proxies: Are Reconstructions of Surface Temperatures Over the Last 1000 Years Reliable? *Annals of Applied Statistics*, **5**, 5-44.

Melvin, T. M., K. R. Briffa, K. Nicolussi and M. Grabner, 2007: Time-varying-response smoothing. *Dendrochronologia*, **25**, 65-69.

Melvin, T. M. and K. R. Briffa, 2008: A "signal-free" approach to dendroclimatic standardisation. *Dendrochronologia*, **26**, 71-86.

Neukom, R., J. Luterbacher, R. Villalba, M. Küttel, D. Frank, P. D. Jones, M. Grosjean, J. Esper, L. Lopez and H. Wanner, 2010: Multi-centennial summer and winter precipitation variability in southern South America. *Geophysical Research Letters*, **37**, DOI: 10.1029/2010GL043680.

Neukom, R. and J. Gergis, 2011: Southern Hemisphere high-resolution palaeoclimate records of the last 2000 years. *The Holocene*, DOI: 10.1177/0959683611427335.

Neukom, R., J. Luterbacher, R. Villalba, M. Kuttel, D. Frank, P. D. Jones, M. Grosjean, H. Wanner, J. Aravena, D. Black, D. Christie, R. D'Arrigo, A. Lara, M. Morales, C. Soliz-Gamboa, A. Srur, R. Urrutia and L. von Gunten, 2011: Multiproxy summer and winter surface air temperature field reconstructions for southern South America covering the past centuries. *Climate Dynamics*, **37**, 35-51.

Newman, L., H. Wanner and T. Kiefer, 2009: Towards a global synthesis of the climate of the last two millenium. *PAGES news*, **17**, 130-131.

Newton, A., R. Thunell and L. Stott, 2006: Climate and hydrographic variability in the Indo-Pacific Warm Pool during the last millennium. *Geophysical Research Letters*, **33**, L19710.

Nunn, P. D., 2000: Environmental catastrophe in the Pacific Islands around A.D. 1300. *Geoarchaeology*, **15**, 715-740.

Nunn, P. D., 2007: The A.D. 1300 event in the Pacific Basin. *The Geographical Review*, **97**, 1-23.

Oppo, D. W., Y. Rosenthal and B. K. Linsley, 2009: 2,000-year-long temperature and hydrology reconstructions from the Indo-Pacific warm pool. *Nature*, **460**, 1113-1116.

Peterson, T. C. and R. S. Vose, 1997: An overview of the global historical climatology network temperature database. *Bulletin of the American Meteorological Society*, **78**, 2837-2849.

Phipps, S., J. Gergis, H. McGregor, A. J. E. Gallant, R. Neukom, S. Stevenson, T. van Ommen, J. Brown, M. Fischer and D. Ackerley, 2012: Palaeoclimate data–model comparison: Concepts and application to the climate of Australasia over the past 1500 years. *Journal of Climate*, in review.

Phipps, S. J., L. D. Rotstayn, H. B. Gordon, J. L. Roberts, A. C. Hirst and W. Budd, 2011: The CSIRO Mk3L climate system model version 1.0 – Part 1: Description and evaluation. *Geoscientific Model Development*, **4**, 483-509.

Pollack, H. N., S. P. Huang and J. E. Smerdon, 2006: Five centuries of climate change in Australia: the view from underground. *Journal of Quaternary Science*, **21**, 701-706.

Power, S., T. Casey, C. Folland, A. Colman and V. Mehta, 1999: Inter-decadal modulation of the impact of ENSO on Australia. *Climate Dynamics*, **15**, 319-324.

Quinn, T., T. Crowley, F. Taylor, C. Henin, P. Joannot and Y. Join, 1998: A multicentury stable isotope record from a New Caledonia coral: Interannual and decadal SST variability in the southwest Pacific since 1657. *Paleoceanography*, **13**, 412-426.

Rayner, N. A., D. E. Parker, E. B. Horton, C. K. Folland, L. V. Alexander, D. P. Rowell, E. C. Kent and A. Kaplan, 2003: Global analyses of sea surface temperature, sea ice, and night marine air temperature since the late nineteenth century. *Journal of Geophysical Research*, **108**, doi:10.1029/2002JD002670.

Rayner, N. A., P. Brohan, D. E. Parker, C. K. Folland, J. J. Kennedy, M. Vanicek, T. J. Ansell and S. F. B. Tett, 2006: Improved Analyses of Changes and Uncertainties in Sea Surface Temperature Measured In Situ since the Mid-Nineteenth Century: The HadSST2 Dataset. *Journal of Climate*, **19**, 446-469.

Robertson, A., J. Overpeck, D. Rind, E. Mosley-Thompson, G. Zielinski, J. Lean, D. Koch, J. Penner, I. Tegen and R. Healy, 2001: Hypothesized climate forcing time series for the last 500 years. *Journal of Geophysical Research*, **106**, doi:10.1029/2000JD900469.

Robock, A., 2000: Volcanic eruptions and climate. *Review of Geophysics*, **38**, 191-219.

Schaefer, J. M., G. H. Denton, M. Kaplan, A. Putnam, R. C. Finkel, D. J. A. Barrell, B. G. Andersen, R. Schwartz, A. Mackintosh, T. Chinn and C. Schlüchter, 2009: High-Frequency Holocene Glacier Fluctuations in New Zealand Differ from the Northern Signature. *Science*, **324**, 622-625.

Scherrer, S. C. and C. Appenzeller, 2006: Swiss Alpine snow pack variability: major patterns and links to local climate and large-scale flow. *Climate Research*, **32**, 187-199.

Schmidt, G. A., J. H. Jungclaus, C. M. Ammann, E. Bard, P. Braconnot, T. J. Crowley, G. Delaygue, F. Joos, N. A. Krivova, R. Muscheler, B. L. Otto-Bliesner, J. Pongratz, D. T. Shindell, S. K. Solanki, F. Steinhilber and L. E. Vieira, 2012: Climate forcing reconstructions for use in PMIP simulations of the Last Millennium (v1.1). *Geoscientific Model Development*, **5**, 185–191.

Steinhilber, F., J. Beer and C. Fröhlich, 2009: Total solar irradiance during the Holocene. *Geophysical Research Letters*, **36**, doi:10.1029/2009GL040142.

Steinhilber, F. and J. Beer, 2011: Solar activity – the past 1200 years. *PAGES News*, **19**, 5–6.

Tudhope, A., C. Chilcott, M. Mc Culloch, E. Cook, J. Chappell, R. Ellam, D. Lea, J. Lough and G. Shimmield, 2001: Variability in the El Nino Southern Oscillation through a glacial-interglacial cycle. *Science*, **291**, 1511-1517.

Urban, F., J. Cole and J. Overpeck, 2000: Influence of mean climate change on climate variability from a 155-year tropical Pacific coral record. *Nature*, **407**, 989-993.

Wahl, E. R., D. M. Anderson, B. A. Bauer, R. Buckner, E. P. Gille, W. S. Gross, M. Hartman and A. Shah, 2010: An archive of high-resolution temperature reconstructions over the past 2+millennia. *Geochemistry Geophysics Geosystems*, **11**, doi:10.1029/2009GC002817.

Xiong, L. and J. Palmer, 2000: Reconstruction of New Zealand Temperature Back to AD 1720 Using Libocedrus Bidwillii Tree rings. *Climatic Change*, **45**, 339-359.

8. Table captions

Table 1. Proxy data network used in the Australasian SONDJF temperature reconstruction. Note that all coral records are averaged over the September–February period.

Table 2. Warmest and coolest decades (top) and non-overlapping 30-year periods (bottom) calculated for the R27, R21, R14 and R4 networks. Average temperature anomalies relative to the 1961–1990 base period are shown in brackets.

Table 3. Correlations between R27 temperature reconstruction and CSIRO Mk3L model ensemble means. Bolded values are significant as determined by a normal distribution white noise p-value, $p<0.05$.

9. Figure captions

Figure 1. Location of the tree ring (green), coral (blue) and ice core (orange) records used in the R27 predictor network (top) and corresponding temporal coverage of proxy records 1000–2001 (bottom). The dashed line encloses the target region of Australasia defined by the domain 0ºS–50ºS, 110ºE–180ºE. Note that multiple climate proxies are available for some sites.

Figure 2. Instrumental (black) and reconstructed (red) September–February HadCRUT3v spatial mean temperature calculated for the Australasian region (110ºE–180ºE, 0º–50ºS) over the 1921–2001 period. 2SE uncertainty intervals of the reconstruction are shaded.

Figure 3. 3000-member temperature reconstruction ensemble (top) with ensemble median RE over verification intervals within the 1921–1990 overlap period (black, middle) and RE of the ensemble mean over 1900–1920 early verification period (red, bottom). Coloured lines represent a percentile grouping of the ensemble members. The area between the black lines encloses all (100%) members; the area between the lowest (1st percentile) and the highest blue lines (99th percentile) encloses 98% of the members and so on. The dark red line represents the median.

Figure 4. Australasian September–January mean temperature reconstruction, A.D. 1000–2001. Solid line represents the 30- year filtered ensemble mean reconstruction based on multivariate principal component regression performed on a 3000- member ensemble. The 95% combined ensemble and calibration uncertainties are denoted by grey shading. Most reliable periods of the reconstruction (as determined by six reconstruction skill and stability metrics) are shown by solid black line with less reliability indicated by the thin black line. Instrumental HADCRUT3v combined land and ocean temperature data over the 1900–2009 period shown in green. All anomalies are calculated relative to a 1961–1990 base period.

Figure 5. Comparison of the Australasian SONDJF ensemble mean temperature reconstruction (solid black line) with solar grand minima (pink shading) and the Southern Hemisphere component of Gao *et al*.'s (2008) global volcanic sulphate aerosol injection dataset (blue). The 95% combined ensemble and calibration reconstruction uncertainties are denoted by grey shading.

Figure 6. Comparison of the 30 year filtered Australasian SONDJF ensemble mean temperature reconstruction (solid black line) with the ensemble mean of three model simulations derived from the CSIRO Mk3L model developed by Phipps *et al*. (2011). The 95% combined ensemble and calibration reconstruction uncertainties are denoted by grey shading. All anomalies are calculated relative to a 1961–1990 base period.

Figure 7. The distribution of the changes in Australasian mean SONDJF temperature between consecutive non-overlapping 50-year periods of a 10,000-year pre-industrial control simulation.

Figure 8. 30-year running correlation between the R27 Australasian temperature reconstruction and a modified version of the McGregor *et al*. (2010) Unified ENSO Proxy (UEP) which excludes Australasian proxies used in the Braganza *et al*. (2009) study.

Table 1. Proxy data network used in the Australasian SONDJF temperature reconstruction. Note that all coral records are averaged over the September–February period.

	Record name	**Archive**	**Start year**	**End year**	**Lon (°E)**	**Lat (°S)**	**Location**	**Proxy variable**	**Reference/s**
1	Mt Read	Tree rings	999	2001	147	42	Australia	Tree ring width	Cook *et al.* (2006)
2	Oroko	Tree rings	999	2001	170	43	New Zealand	Tree ring width	Cook *et al.* (2006)
3	Palmyra	Coral	1149	1998	162	6	Northern Line Ids	δ18O	Cobb *et al.* (2003)
4	Celery Top Pine East	Tree rings	1430	1994	148	42	Australia	Tree ring width	Allan *et al.* (2001)
5	Pink Pine South Island composite	Tree rings	1457	1999	172	42	New Zealand	Tree ring width	Duncan *et al.* (2010)
6	Urewera	Tree rings	1462	1987	177	39	New Zealand	Tree ring width	Xiong and Palmer (2000)
7	Buckley's Chance	Tree rings	1463	1991	146	42	Australia	Tree ring width	Buckley *et al.*(1997)
8	North Island_LIBI_Composite_1	Tree rings	1526	1992	175	39	New Zealand	Tree ring width	Xiong and Palmer (2000)
9	Takapari	Tree rings	1533	1992	176	40	New Zealand	Tree ring width	Xiong and Palmer (2000)
10	Mangawhero	Tree rings	1551	1994	175	39	New Zealand	Tree ring width	D'Arrigo *et al.* (1998; 2000)
11	Kauri	Tree rings	1577	2002	174	36	New Zealand	Tree ring width	Fowler *et al.*(2008)
12	Fiji_AB	Coral	1617	2001	179	17	Fiji	δ18O	Linsley *et al.* (2006)
13	NI_LIBI_Composite_2	Tree rings	1651	1990	174	39	New Zealand	Tree ring width	Xiong and Palmer (2000)
14	New_Caledonia	Coral	1658	1992	166	22	New Caledonia	δ18O	Quinn *et al.* (1998)
15	Stewart_Island_HABI_composite	Tree rings	1758	1993	168	47	New Zealand	Tree ring width	D'Arrigo *et al.* (1996; 1998; 2000)
16	Rarotonga	Coral	1761	1996	160	21	Cook Islands	18O	Linsley *et al.* (2006; 2008)
17	Vostok	Ice core	1774	1999	107	78	Antarctica	δ18O	Ekaykin *et al.* (2004)
18	Vostok	Ice core	1774	1999	107	78	Antarctica	Accumulation	Ekaykin *et al.* (2004)
19	Fiji	Coral	1780	1997	179	17	Fiji	δ18O	Linsley *et al.* (2004)
20	Bali	Coral	1783	1989	115	8	Indonesia	δ18O	Charles *et al.*(2003)
21	Abrolhos	Coral	1794	1993	114	28	Australia	δ18O	Kuhnert *et al.* (1999)
22	Maiana	Coral	1840	1994	173	1	North Gilbert Ids	δ18O	Urban *et al.* (2000)
23	Bunaken	Coral	1863	1990	123	3	Indonesia	δ18O	Charles *et al.*(2003)
24	Rarotonga.3R	Coral	1874	2000	160	21	Cook Islands	δ18O	Linsley *et al.* (2006; 2008)
25	Ningaloo	Coral	1878	1995	114	22	Australia	δ18O	Kuhnert *et al.* (2000)
26	Madang	Coral	1880	1993	146	5	Papua New Guinea	δ18O	Tudhope *et al.* (2001)
27	Laing	Coral	1884	1993	145	4	Papua New Guinea	δ18O	Tudhope *et al.* (2001)

Table 2. Warmest and coolest decades (top) and non-overlapping 30-year periods (bottom) calculated for the R27, R21, R14 and R4 temperature proxy networks. Average temperature anomalies relative to the 1961–1990 base period are shown in brackets.

Decades (Start year indicated)

	R27	R21	R14	R4
Warmest decade	1990 (+0.11)	1990 (+0.11)	1990 (+0.15)	1990 (+0.12)
2nd warmest	1980 (+0.11)	1980 (+0.10)	1980 (+0.10)	1980 (+0.08)
3rd warmest	1970 (+0.02)	1970 (+0.03)	1970 (-0.00)	1970 (-0.01)
4th warmest	1240 (-0.01)	1240 (-0.02)	1240 (-0.02)	1240 (-0.01)
5th warmest	1330 (-0.02)	1330 (-0.03)	1330 (-0.03)	1330 (-0.03)
Coldest decade	1830 (-0.47)	1830 (-0.47)	1520 (-0.45)	1320 (-0.41)
2nd coldest	1840 (-0.47)	1840 (-0.46)	1830 (-0.44)	1730 (-0.40)
3rd coldest	1520 (-0.45)	1520 (-0.45)	1650 (-0.44)	1060 (-0.40)
4th coldest	1650 (-0.44)	1760 (-0.43)	1680 (-0.42)	1830 (-0.40)
5th coldest	1900 (-0.44)	1650 (-0.43)	1320 (-0.40)	1520 (-0.39)

Non-overlapping 30-year periods

	R27	R21	R14	R4
Warmest	1971-2000 (+0.09)	1971-2000 (+0.09)	1971-2000 (+0.10)	1971-2000 (+0.07)
2nd warmest	1238-1267 (-0.09)	1238-1267 (-0.09)	1238-1267 (-0.09)	1238-1267 (-0.09)
3rd warmest	1330-1359 (-0.10)	1330-1359 (-0.11)	1330-1359 (-0.11)	1330-1359 (-0.10)
Coldest	1830-1859 (-0.44)	1829-1858 (-0.43)	1634-1663 (-0.40)	1828-1859 (-0.38)
2nd coldest	1634-1663 (-0.40)	1634-1663 (-0.40)	1829-1858 (-0.39)	1056-1085 (-0.37)
3rd coldest	1884-1913 (-0.38)	1056-1085 (-0.36)	1056-1085 (-0.36)	1886-1915 (-0.36)

Table 3. Correlations between R27 temperature reconstruction and CSIRO Mk3L model ensemble means. Bolded values are significant as determined by a normal distribution white noise p-value, $p<0.05$.

Interval	Inter-annual correlation	30-year filtered correlation
1000–2000	**0.27**	**0.33**
1000–1300	-0.04	-0.01
1301–1600	0.09	**0.15**
1601–1900	**0.18**	**0.27**
1901–2000	**0.77**	**0.90**

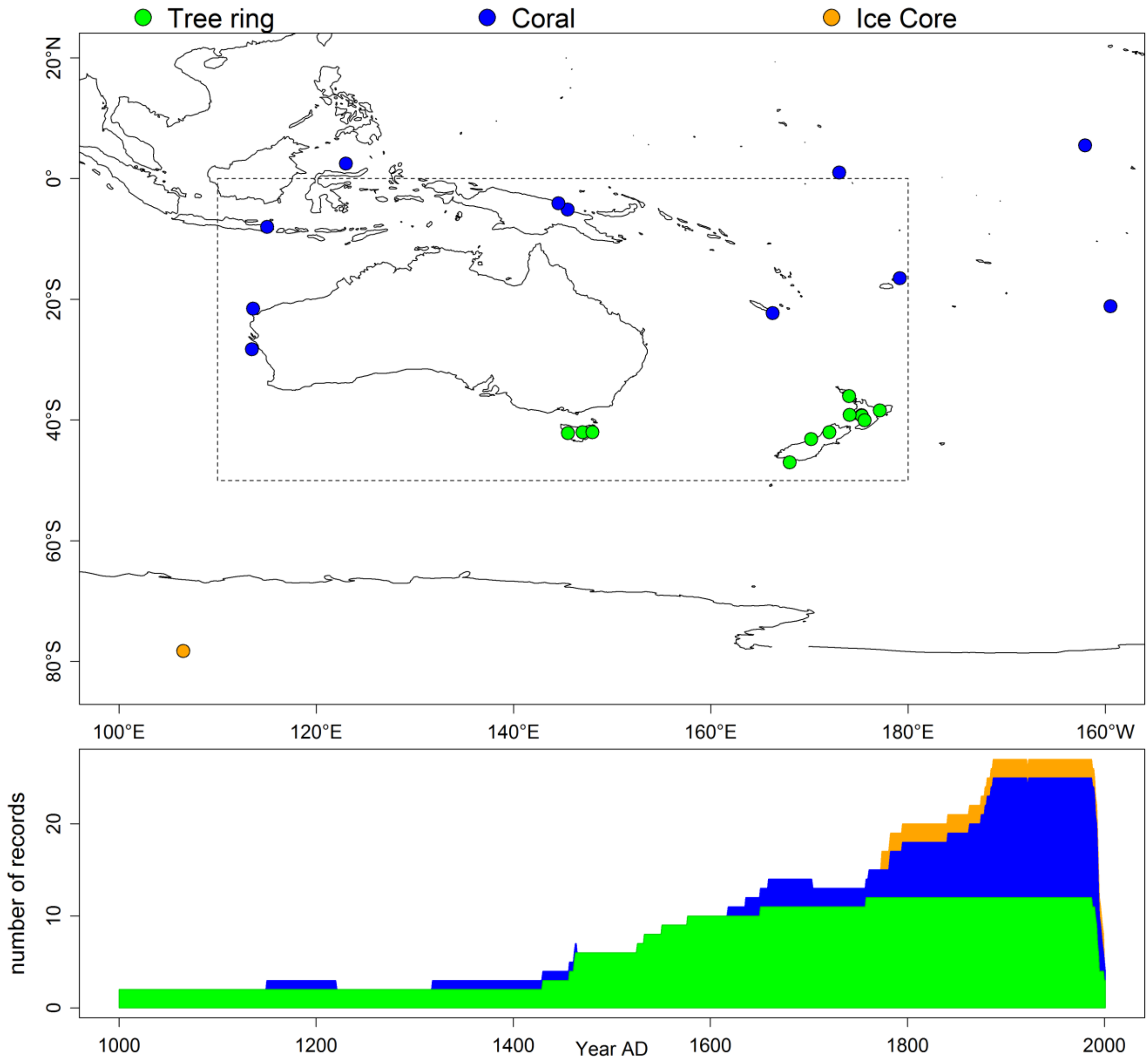

Figure 1. Location of the tree ring (green), coral (blue) and ice core (orange) records used in the R27 predictor network (top) and corresponding temporal coverage of proxy records 1000–2001 (bottom). The dashed line encloses the target region of Australasia defined by the domain 0ºS–50ºS, 110ºE–180ºE. Note that multiple climate proxies are available for some sites.

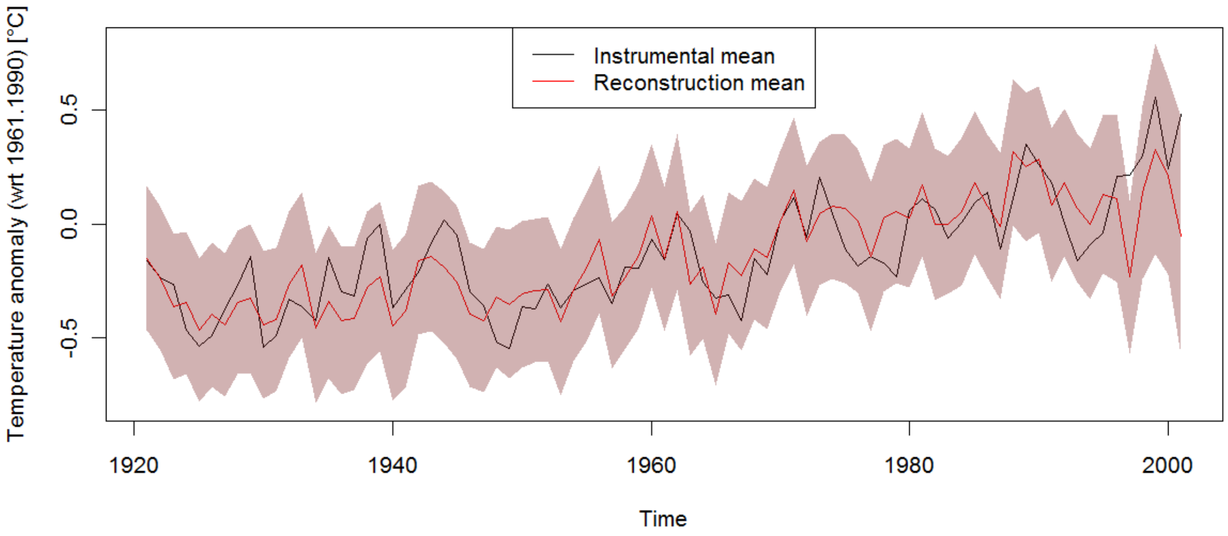

Figure 2. Instrumental (black) and reconstructed (red) September–February HadCRUT3v spatial mean temperature calculated for the Australasian region (110ºE–180ºE, 0º–50ºS) over the 1921–2001 period. 2SE uncertainty intervals of the reconstruction are shaded.

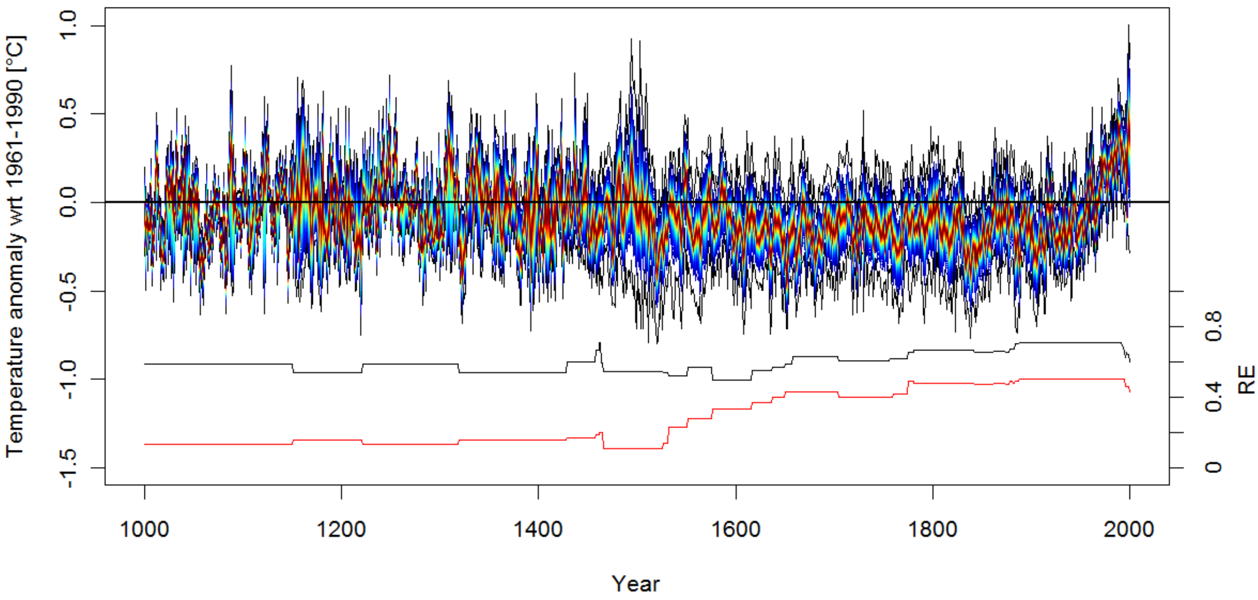

Figure 3. 3000-member temperature reconstruction ensemble (top) with ensemble median RE over verification intervals within the 1921–1990 overlap period (black, middle) and RE of the ensemble mean over 1900–1920 early verification period (red, bottom). Coloured lines represent a percentile grouping of the ensemble members. The area between the black lines encloses all (100%) members; the area between the lowest (1st percentile) and the highest blue lines (99th percentile) encloses 98% of the members and so on. The dark red line represents the median.

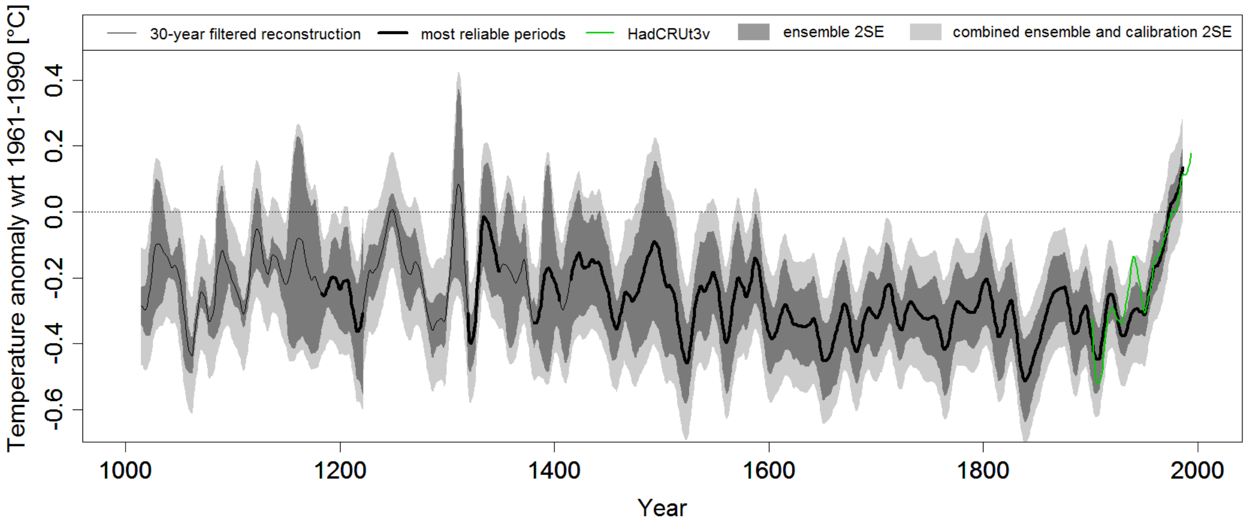

Figure 4. Australasian September–January mean temperature reconstruction, A.D. 1000–2001. Solid line represents the 30- year filtered ensemble mean reconstruction based on multivariate principal component regression performed on a 3000- member ensemble. The 2SE combined ensemble and calibration uncertainties are denoted by grey shading. Most reliable periods of the reconstruction (as determined by eight reconstruction skill and stability metrics) are shown by solid black line with less reliability indicated by the thin black line. Instrumental HADCRUT3v combined land and ocean temperature data over the 1900–2009 period shown in green. All anomalies are calculated relative to a 1961–1990 base period.

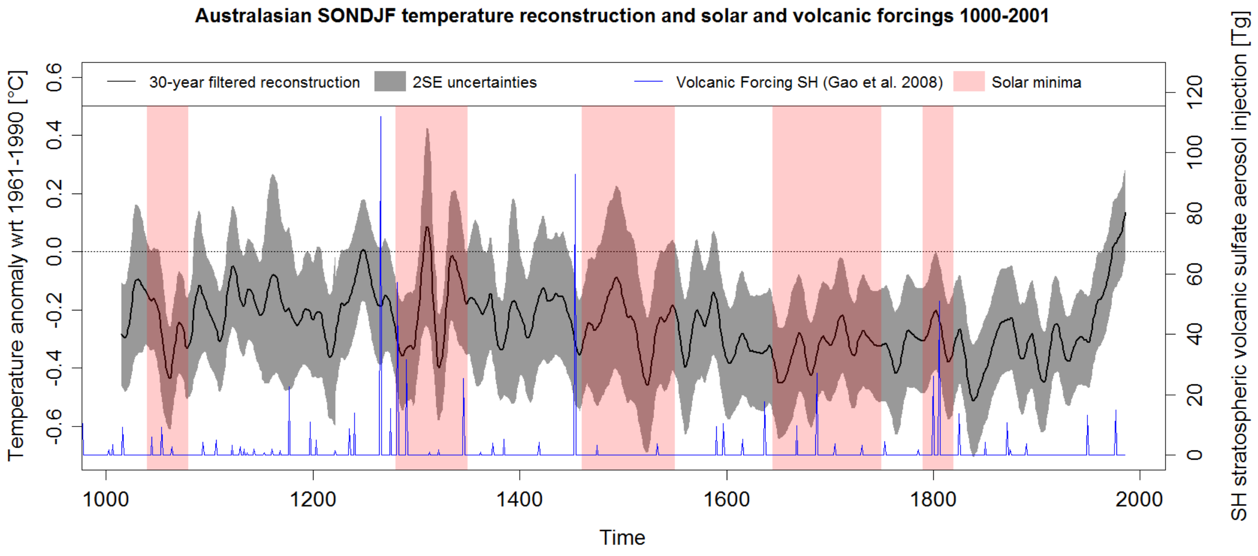

Figure 5. Comparison of the Australasian SONDJF ensemble mean temperature reconstruction (solid black line) with solar grand minima (pink shading) and the Southern Hemisphere component of Gao *et al.*'s (2008) global volcanic sulphate aerosol injection dataset (blue). The 2SE combined ensemble and calibration reconstruction uncertainties are denoted by grey shading.

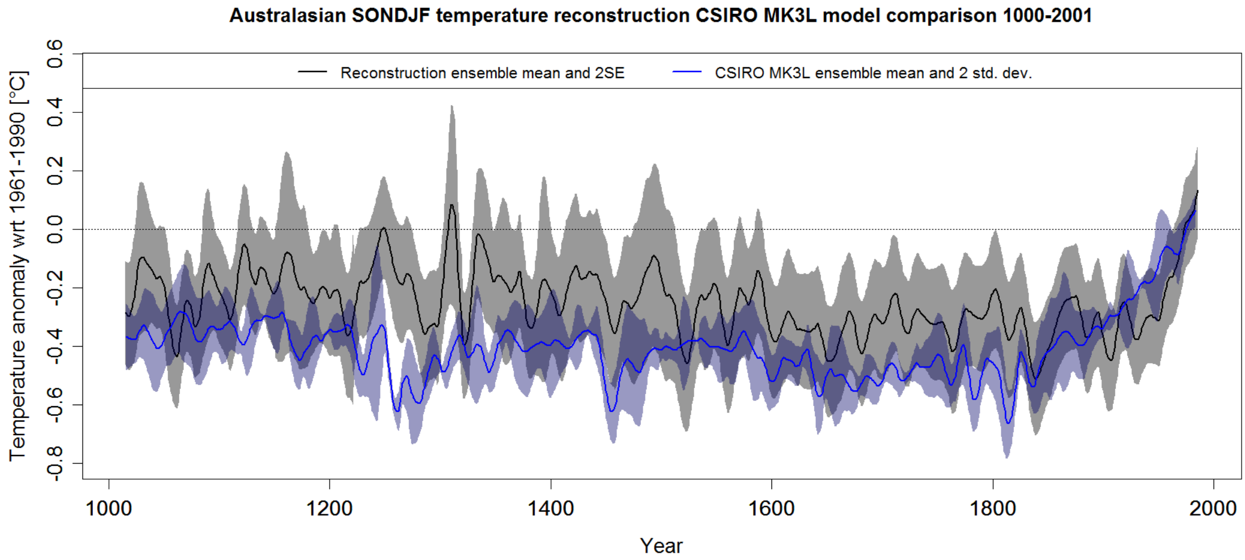

Figure 6. Comparison of the 30 year filtered Australasian SONDJF ensemble mean temperature reconstruction (solid black line) with the ensemble mean of three model simulations derived from the CSIRO Mk3L model developed by Phipps *et al*. (2011). The 2SE combined ensemble and calibration reconstruction uncertainties are denoted by grey shading. All anomalies are calculated relative to a 1961–1990 base period.

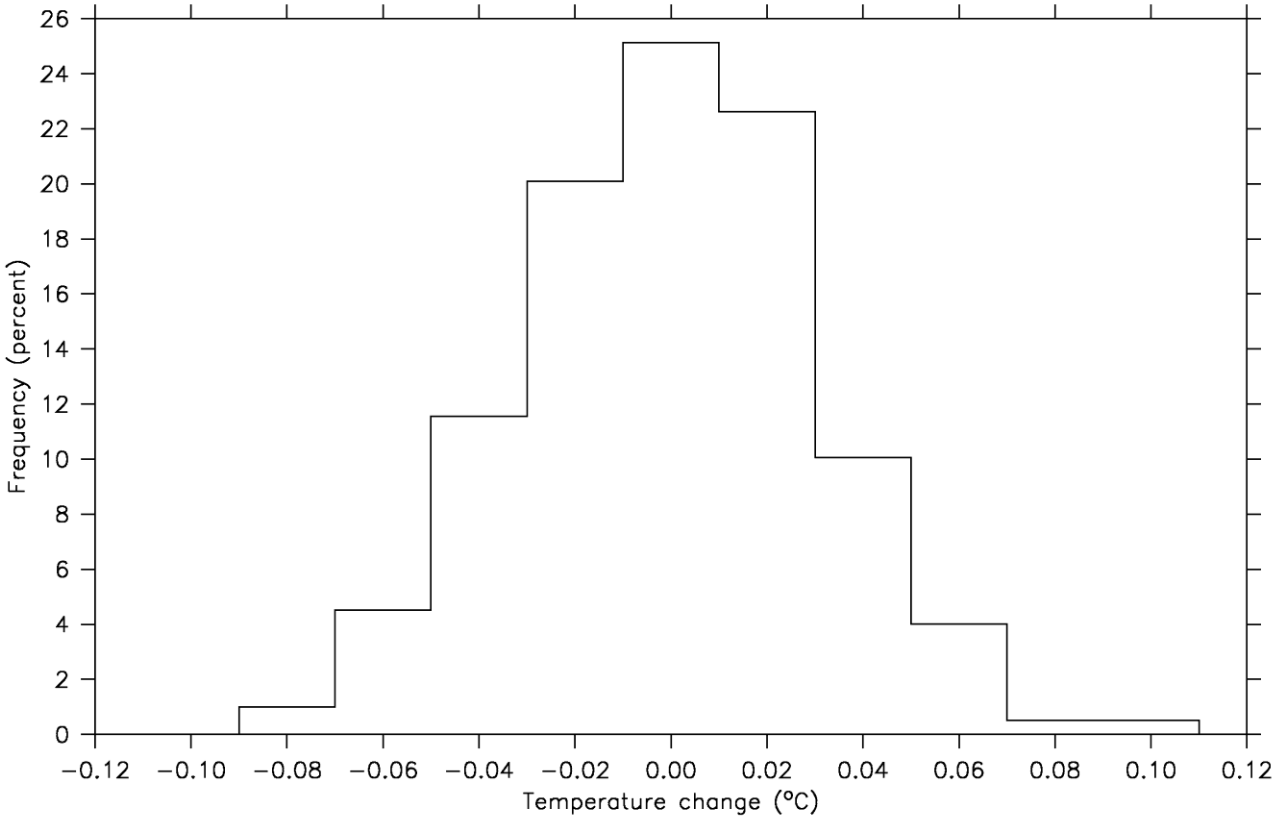

Figure 7. The distribution of the changes in Australasian mean SONDJF temperature between consecutive non-overlapping 50-year periods of a 10,000-year pre-industrial control simulation.

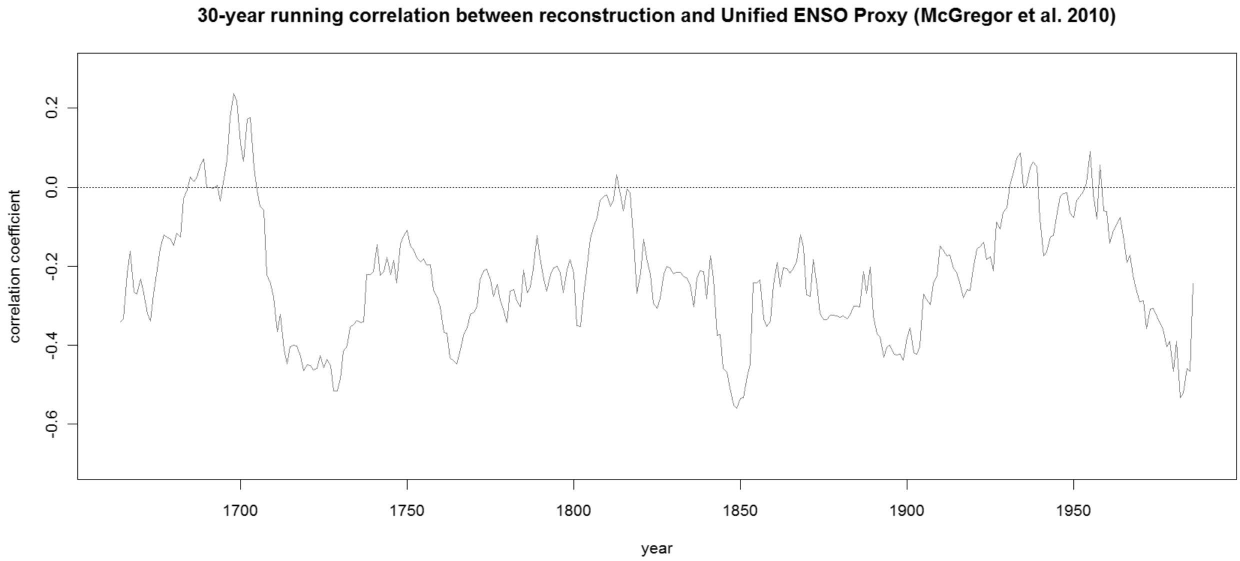

Figure 8. 30-year running correlation between the R27 Australasian temperature reconstruction and a modified version of the McGregor *et al*. (2010) Unified ENSO Proxy (UEP) which excludes Australasian proxies used in the Braganza *et al*. (2009) study. Note that negative UEP values correspond to La Niña-like conditions and vice versa.